PONTIFICIA UNIVERSIDAD CATÓLICA DE CHILE
ESCUELA DE INGENIERÍA

THEORETICAL AND EXPERIMENTAL ANALYSIS OF THE BEARING CAPACITY OF SHALLOW FUNDATIONS ON COHESIONLESS SOILS

Thesis submitted of the office of Research and Graduate Studies in fulfillment of the requirements for the Degree of Master of Sciences in Civil Engineering by

FELIPE ALBERTO VILLALOBOS JARA

Santiago de Chile, December 2000

PONTIFICIA UNIVERSIDAD CATÓLICA DE CHILE
ESCUELA DE INGENIERÍA
Departamento de Ingeniería Estructural y Geotécnica

THEORETICAL AND EXPERIMENTAL ANALYSIS OF THE BEARING CAPACITY OF SHALLOW FUNDATIONS ON COHESIONLESS SOILS

FELIPE ALBERTO VILLALOBOS JARA

Members of the Graduate Committee:

Prof. Dr. FERNANDO RODRÍGUEZ

Prof. Dr. RAMÓN VERDUGO

Prof. Dr. JORGE TRONCOSO

Santiago de Chile, December 2000

ABSTRACT

In the present study, it was carried out a theoretical and experimental investigation of the bearing capacity of shallow foundations on cohesionless soil. The purpose was to improve the current state of the knowledge about the existing computational procedures to predict its magnitude. The technical literature gives diverse semi-empirical formulae to evaluate the parameter N_γ. Nevertheless, they have great differences between them. The theme interests specially in Chile because there are important cities like: Valparaíso, Concepción and Viña del Mar, wherein sandy soils abound. Therefore, any advance in this field will undoubtedly result in major safety and economy of the structures that could be build over this kind of soil in the future.

To examine the existing theories with a critical point of view the investigation was subdivided in four parts. In the first, the pertinent bibliography was reviewed. In the second, the theories of bearing capacity, based in the plasticity theory were assessed. The object of the third part was to elaborate a procedure to experimentally determine the real bearing capacity of small-scale shallow footings. And finally, the fourth part of the investigation was to carry out a series of plate-load tests on sand.

It was necessary to design and build an equipment to make an homogeneous sample of sand of large dimensions. In addition, a controlled vertical load system had to be developed. To avoid boundary effects from the testing tank, the width of the plates ranged from 5 to 10cm for modelling plane strain and axisymmetric problems.

It may be drawn from the experimental results that Terzaghi`s theory gives, in general, a better prediction than the theories of Vesic, Hansen and Meyerhof.

ACKNOWLEDGEMENTS

I would like to thank Professor Dr. Fernando Rodríguez, for proposing the research theme, for the supervision and advice.

The research presented in this thesis would not have been possible without the encouragement and constructive advice offered by Professor Dr. Ramón Verdugo.

I am also very grateful to the technical staff of the DICTUC S.A., especially Mr. Manuel Ravello, Mr. Atilio Muñoz, and Mr. Jonathan Miranda, who helped me during the experimental stages of this study. I would also like to acknowledge Ingrid Luaiza, Juan Velásquez, Marcelo Morales, Andres Muñoz and Leonardo Lizama from the laboratory and Mrs. Miriam Fredes from the secretary's office. They gave me a very friendly and nice atmosphere within the research activities.

It is appropriate to also thank friends and colleagues. Sergio Barrera helped me in the revision and correction of this English version. Fernando Vielma was very interested in bearing capacity and other geotechnical and not geotechnical issues. Gastón Oróstegui, for his aid when needed.

I am grateful for the funding for this research project which was obtained by Prof. Rodríguez from the National Funding for the Technological and Scientific Research FONDECYT (grant number 1990116). I also acknowledge a scholarship given by the Faculty of Engineering of the PUC.

TABLE OF CONTENTS

LIST OF TABLES

LIST OF FIGURES

I. INTRODUCTION

The bearing capacity study of shallow footings is a subject with a very long reference list. The basic structure of formulae used for calculations of bearing capacity today, however, is no different from that proposed by Terzaghi in 1943. The first important contributions are due to Prandtl (1921) and Reissner (1924), who considered a punch over a weightless semi-infinite space, and Sokolovski (1965), in regard to a ponderable soil, all under plane strain conditions.

The ultimate bearing capacity of shallow strip footings is generally determined by the Terzaghi method (1943). Terzaghi's equation is an approximate solution which uses the superposition technique to combine the effects of cohesion c, soil weight γ and surcharge q. This contributions are expressed through three factors of bearing capacity, N_c, N_γ y N_q. These bearing capacity factors are functions of angle of internal friction ϕ. Terzaghi (1943) used an approximate approach to the physical reality where only a global limit equilibrium of rigid blocks defined by the Prandtl failure mechanism was required, but considering the basal angle of the central wedge equal to ϕ, instead of $45^o + \phi/2$.

Meyerhof (1951) obtained, with a similar technique of the Terzaghi's approach, approximate solutions to the plastic equilibrium of shallow foundations and deep foundations, assuming a different failure mechanism and like Terzaghi, expressing the results in the form of bearing capacity factors in terms of the angle of internal friction ϕ.

In general, the majority of the authors coincide in the expressions employed to determine N_c y N_q, nevertheless, there is a great discrepancy with respect to the values of the factor N_γ. This is the principal reason that encouraged the present investigation.

This investigation is part of a bearing capacity of shallow foundations on sand study more extensive. Thus this thesis constitute a part of the investigation that involve the experimental data acquisition with scale footings. Thereafter it will be calibrate finite element

models based in new constitutive laws of sandy soils currently in course inside the project FONDECYT Nº 1990116.

Therefore the objectives of this thesis are expand the experimental data base of bearing capacity tests on sand, particularly for internal friction angles greater than 40º due to for this range the information is scarce and the major differences in values of N_γ are found.

As a further objective, this study makes a critical revision of the classical bearing capacity theories in the light of the experimental results here obtained.

II. BEARING CAPACITY OF SANDY SOILS.

2.1 Bearing Capacity Factors

2.1.1 Bearing capacity of a weightless half-space.

Prandtl in 1921 considered a rigid-perfectly plastic half space loaded by a strip punch. The failure criterion of the material was described by the Mohr-Coulomb function, which in the plane case presents the following expression:

$$f(\sigma_x,\sigma_z,\tau_{xz}) = (\sigma_x+\sigma_z)\,\mathrm{sen}\phi - \sqrt{(\sigma_x-\sigma_z)^2+4\tau_{xz}^2} + 2c\cos\phi = 0 \qquad (2.1)$$

where ϕ is the internal friction angle, and c is the cohesion. Equation (2.1), along with two differential equations of equilibrium, in plane deformation, leads to a set of hyperbolic-type differential equations, often referred to as Kötter equations (Kötter, 1903). Prandtl's stress boundary condition was zero traction on the surface of the half space, except for the strip punch where the pressure was unknown. The classical Prandtl mechanism is shown on the figure 2.1. A closed-form solution to the failure pressure, q', under the strip was found by Prandtl to be

$$q' = c\left[tan^2\left(\frac{\pi}{4}+\frac{\phi}{2}\right)e^{\pi tan\phi} - 1\right]\cot\phi \qquad (2.2)$$

Subsequently, Reissner (1924) considered a similar problem. The material was regarded as purely frictional (c = 0), and the surface of the half-space (except for the strip punch) was loaded by a uniformly distributed pressure q. The solution of the hyperbolic-type equations for the new boundary conditions and no cohesion led Reissner to the following limit pressure

$$q'' = qtan^2\left(\frac{\pi}{4}+\frac{\phi}{2}\right)e^{\pi tan\phi} \qquad (2.3)$$

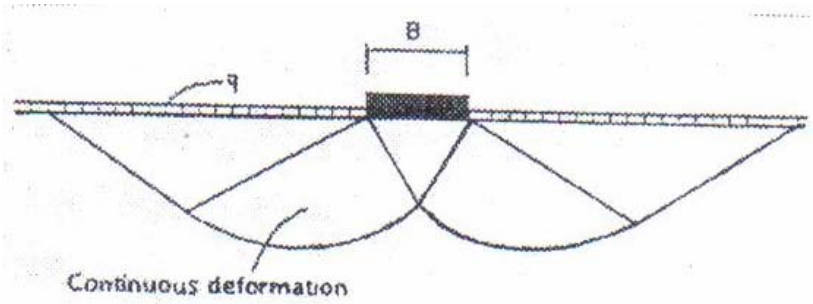

Figure 2.1: Prandtl mechanism; original mechanism with continual deformation and the rigid-block collapse pattern.

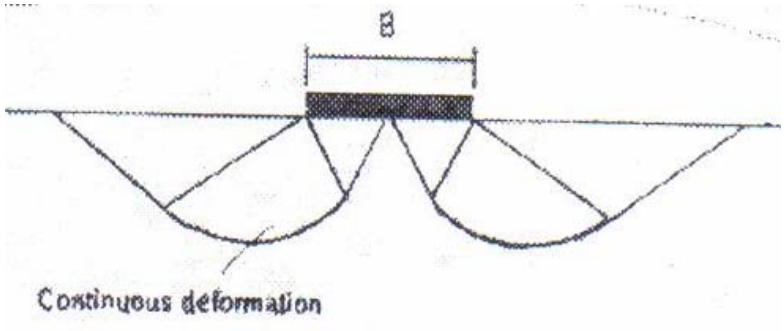

Figure 2.2: Hill mechanism of collapse under a smooth loaded strip.

Solving the equations simultaneously for a frictional-cohesive material and boundary condition q, one obtains exactly the same slip-line field, and applying the principle of superposition the result can be written as

$$q = q' + q'' = cN_c + qN_q \qquad (2.4)$$

where

$$N_c = (N_q - 1)\cot\phi \qquad \text{and} \qquad N_q = \tan^2\left(\frac{\pi}{4} + \frac{\phi}{2}\right)e^{\pi\tan\phi} \qquad (2.5)$$

The solution with the bearing capacity factors in equation (2.5) is, indeed, the exact solution from the theoretical point of view and is adopted today in most bearing capacity formulae.

Hill proposed in 1950 a different mechanism of failure for a punch-indentation problem over a weightless rigid-plastic half-space (figure 2.2). If a smooth foundation and a weightless soil is considered, the coefficients N_c and N_q based on the Hill mechanism are identical to those in equation (2.5). The extent of this mechanism, however, is considerably smaller, which substantially affects the influence of the self-weight for ponderable soils. The difference between the both ultimate load is significant, if it compares with the load obtained by the Prandtl mechanism.

2.1.2 Weight soil inclusion in the ultimate bearing capacity.

Sokolovski in 1965 used the method of characteristics for weighted soils. It was used earlier by Lundgren and Mortensen in 1953, to estimate the influence of γ on bearing capacity. The differential equations of characteristics for the case where $\gamma > 0$ are identical to those for a weightless soil, but the relations along slip lines differ. Consequently, the solution cannot be obtained in a closed form, and the contributions related to cohesion c, boundary condition q, and the soil weight γ cannot be separated.

Terzaghi's bearing capacity formula (1943) for strip foundations is widely used. It is commonly described as a sum of the terms (equation 2.4) plus another term depending on specific weight of the soil γ

$$q_u = cN_c + \gamma D_f N_q + \frac{1}{2}\gamma B N_\gamma \qquad (2.6)$$

where q_u is the ultimate bearing capacity; B and D_f are the footing width and the embedded depth of the footing.

For N_γ several formulae have been proposed by many researchers, as cited by Zadoroga (1994). Vesic in 1973 recommended using the bearing capacity factor proposed by Caquot y Kérisel in 1953, which can be approximated by

$$N_\gamma = 2(N_q + 1)\tan\phi \qquad (2.7)$$

Meyerhof proposed in 1951 the following formula

$$N_\gamma = (N_q - 1)\tan(1.4\phi) \qquad (2.8)$$

Brinch Hansen (1970) presented the following expression

$$N_\gamma = 1.5(N_q - 1)\tan\phi \qquad (2.9)$$

The figure 2.3 plots N_γ in semi logarithmic scale for the most interesting internal friction angle ϕ. Respectively, there is no doubt that the most significant differences for N_γ, according to various authors, become greater as the friction angle ϕ increases beyond 30º. For example, when $\phi = 48º$, $N_\gamma = 369$, using the B. Hansen (1970) formula, and $N_\gamma = 526$ using the Meyerhof formula, i.e. a difference of the about 40%.

Bearing capacity factors N_c y N_q are functions of the angle of internal friction ϕ and are independent of footing width B in the formulae as shown by equations (2.2) - (2.5); however, the bearing capacity factor N_γ calculated from the loading tests of footings on sand grounds reduces with increasing footing size until a certain value, becoming stabilized later (De Beer, 1970; Kusakabe et al., 1992 and Ueno et al., 1998). This phenomenon is referred to as the size effects of footing width on the bearing capacity factor N_γ. It is, therefore, important to clarify the mechanism of size effects and developed a rational calculation method for the bearing capacity of footings.

2.1.3 Bearing capacity calculation.

There is currently a general expression to estimate the ultimate load of shallow footings under vertical and central load

$$q_u = s_c d_c\, cN_c + s_q d_q\, \gamma D_f N_q + s_\gamma d_\gamma \frac{1}{2} \gamma B N_\gamma \qquad (2.10)$$

where s_c, s_q and s_γ are footing shape factors

and d_c, d_q and d_γ are depth factors.

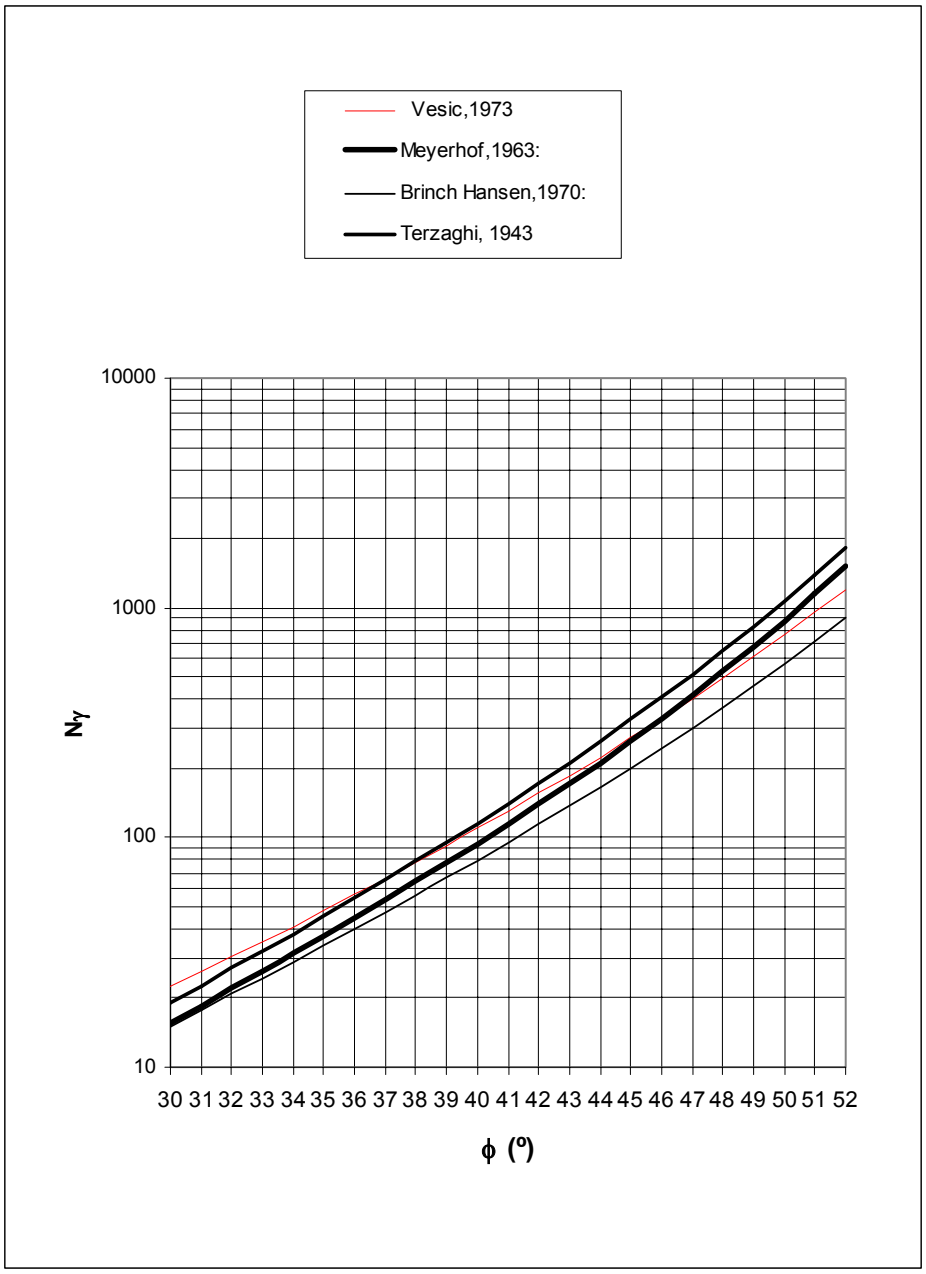

Figure 2.3: Bearing capacity factor N_γ versus ϕ.

The tables 2.1, 2.2, 2.3 and 2.4 show the shape and depth factors obtained by Terzaghi (1943), Meyerhof (1963), Brinch Hansen (1970) and Vesic (1973). This equations where developed for the analysis of shallow foundations.

It can see in table 2.1 that Terzaghi only used shape factors with the cohesion (s_c) and base (s_γ) terms. There is no consideration of depth factors.

Table 2.1: Terzaghi's shape factors (1943).

	strip	round	square
s_c	1.0	1.3	1.3
s_γ	1.0	0.6	0.8

Meyerhof (1951) included a shape factor s_q with the depth term N_q. The shape and depth factors in table 2.2 are from Meyerhof (1963) and are somewhat different from his 1951 values. The shear effect along the failure line was still being ignored, Meyerhof proposed depth factors d_c, d_q and d_γ.

Brinch Hansen proposed in 1970 his general bearing capacity case. Hansen's shape, depth and other factors making up the general bearing capacity equation are given in table 2.3. These represent revisions and extensions from earlier proposals in 1957 and 1961.

The Vesic (1973) procedure is essentially the same as the method of Brinch Hansen with select changes. There are differences in the s_q term as in table 2.4.

Table 2.2: Meyerhof's shape and depth factors (1963).

Factors	*Value*	*for*
Shape	$s_c = 1+0.2K_p \frac{B}{L}$	any ϕ
	$s_q = s_\gamma = 1+0.1K_p \frac{B}{L}$	$\phi > 10^o$
	$s_q = s_\gamma = 1$	$\phi = 0$
Depth	$d_c = 1+0.2\sqrt{K_p}\ \frac{D_f}{L}$	any ϕ
	$d_q = d_\gamma = 1+0.1\sqrt{K_p}\ \frac{D_f}{L}$	$\phi > 10^o$
	$d_q = d_\gamma = 1$	$\phi = 0$

Where $K_p = \tan^2(45 + \frac{\phi}{2})$; (B,L) = width and length of the footing.

Table 2.3: Hansen's shape and depth factors (1970).

Shape factors		Depth factors	
$s_c' = 0.2\frac{B'}{L'}$	$\phi = 0^o$	$d_c' = 0.4k$	$\phi = 0^o$
		$d_c = 1.0 + 0.4k$	
$s_c = 1.0 + \frac{N_q}{N_c}\cdot\frac{B'}{L'}$		$k = \frac{D_f}{B}$	for $\frac{D_f}{B} \le 1$
$s_c = 1.0$ for strip footing		$k = \arctan\left(\frac{D_f}{B}\right)$	for $\frac{D_f}{B} > 1$
		(k in radians)	
$s_q = 1.0 + \frac{B'}{L'}\text{sen}\phi$	for every ϕ	$d_q = 1 + 2\tan\phi(1-\text{sen}\phi)^2 k$	
$s_\gamma = 1.0 - 0.4\frac{B'}{L'}$	≥ 0.6	$d_\gamma = 1.0$	for every ϕ

Note use of "effective" base dimensions B' and L'.

The values above are applicable for only vertical load.

Table 2.4: Vesic's shape and depth factors (1973).

Shape factors	Depth factors
$s_c = 1.0 + \frac{N_q}{N_c} \cdot \frac{B}{L}$	$d_c = 1.0 + 0.4k$
$s_c = 1.0$ for strip footing	$k = \frac{D_f}{B}$ for $\frac{D_f}{B} \leq 1$
	$k = \arctan\left(\frac{D_f}{B}\right)$ for $\frac{D_f}{B} > 1$
	(k in radians)
$s_q = 1.0 + \frac{B}{L}\tan\phi$ for every ϕ	$d_q = 1 + 2\tan\phi(1-\text{sen}\phi)^2 k$
$s_\gamma = 1.0 - 0.4\frac{B}{L} \geq 0.6$	$d_\gamma = 1.0$ for every ϕ

2.1.4 Comparative analysis of the bearing capacity formulae.

Changes in the stress-strain behaviour of sand in triaxial tests due to changes in relative density are well known (figure 2.4). Dense sands expand during shear, loose sands compress. Similar changes take place as stress levels increase. Sands of the same initial relative density expand at low stresses and compress at high stresses.

To illustrate this behaviour difference between a loose sand and other dense sand, it will be considered as follows the bearing capacity of two strip shallow footings. The width are B = 7.62cm and B = 15.24cm. The angles of internal friction of the sand used are $\phi = 34^\circ$ and $\phi = 43^\circ \pm 0.5^\circ$. Five different methods to compute the ultimate bearing capacity are applied. To calculate the ultimate bearing capacity with the stress characteristic method it assumed that the footings base are smooth.

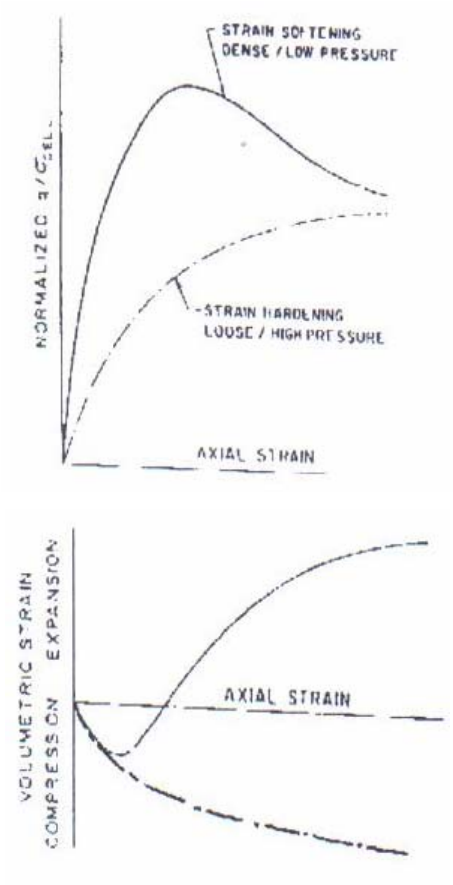

Figure 2.4: Typical curves of stress-strain behaviour and volume change for sands. (Graham and Hovan, 1986).

Table 2.5: Ultimate Bearing Capacity, q_u (kg/cm^2), γ = 1.620T/m^3, D_f = 0 and ϕ = 34º.

B (cm)	*Characteristic Stress method(*)*	*Meyerhof*	*B. Hansen*	*Vesic*	*Terzaghi (rough plate)*
7.62	0.09	0.19	0.18	0.25	0.23
15.24	0.19	0.38	0.36	0.51	0.47

(*) : After Ko and Davidson (1973).

The table 2.5 shows the results obtained for the sand with ϕ = 34º, where it can see the important differences of each method. Attention must being paid to the great discrepancy among the characteristic stress method and the others. On the other hand, the ultimate load is directly proportional to the width *B*.

Given the great sensibility for higher values of the angle of internal friction ϕ, the results of the factor N_γ obtained for a sand with ϕ varying between 42.5º and 43.5º are shown in the table 2.6. The values found confirm the importance of the well determination of ϕ, in a more accurate way. Variations verified for the ultimate load are smaller due to little changes of this angle. Moreover, the characteristic stress method newly gives results clearly lower.

Table 2.6: Ultimate Bearing Capacity, q_u (kg/cm^2), γ = 1.750T/m^3, D_f = 0.

ϕ (º)	*B (cm)*	*Characteristic Stress method(*)*	*Meyerhof*	*B. Hansen*	*Vesic*	*Terzaghi (rough plate)*
42.5	7.62	0.60	1.03	0.83	1.14	1.27
42.5	15.24	1.10	2.06	1.67	2.27	2.54
43	7.62	0.66	1.14	0.91	1.24	1.41
43	15.24	1.22	2.28	1.83	2.49	2.82
43.5	7.62	0.73	1.27	1.00	1.36	1.56
43.5	15.24	1.34	2.53	2.00	2.73	3.13

(*) : After Ko and Davidson (1973).

2.2 Variation of the angle of internal friction according to the tensional state.

The angle of internal friction that there should be employed in the traditional bearing capacity formulae it should be the plain strain angle of shearing resistance, since this was the original calculation hypothesis.

It is commonly known that plane strain angles of shearing resistance ϕ_p in a given sand are larger than corresponding values ϕ_{tx} obtained from axially symmetric triaxial tests, and as it was said before, in particular to higher values of ϕ, a little change in ϕ can affect extraordinarily the results.

Figure 2.5 shows the three published relationships between ϕ_p and ϕ_{tx} in function of the porosity (Graham and Hovan, 1986). In the present study of surface footings the relationship by Bishop (1966) was used in the following forms:

(i) for $\phi_{tx} < 33^o$, $\phi_p = \phi_{tx}$;

(ii) for $33^o \leq \phi_{tx} < 36^o$,

$$\ln\phi_p = 1.666\ln\phi_{tx} - 2.336 \qquad (2.11)$$

(iii) for $36^o \leq \phi_{tx}$,

$$\ln\phi_p = 1.293\ln\phi_{tx} - 1.002$$

This analytical expressions have been drawn in the figure 2.6.

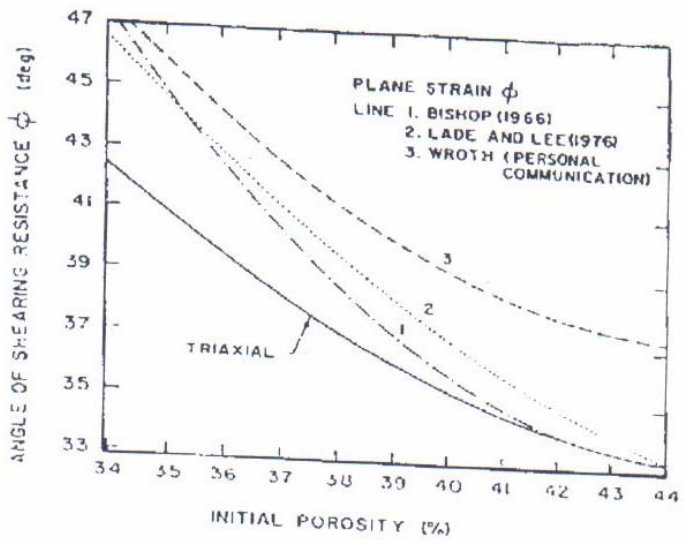

Figure 2.5: Experimental relationships between triaxial and plain strain friction angles. (Graham and Hovan, 1986).

On the other hand, in reality the strength Mohr-Coulomb envelope is not straight but curved, so ϕ is not constant. This is more manifest for higher confinement tensions. Which is caused principally for the particles ruptures with the increase of the confinement tensions.

Furthermore the curvature is due to changes with pressure level in the relative magnitudes of three components of sand strength: sliding friction, particle rearrangement, and dilatancy (Graham and Hovan, 1986). Figure 2.7 shows the failure envelope, where the angle of shearing resistance ϕ is constant for a typical sand.

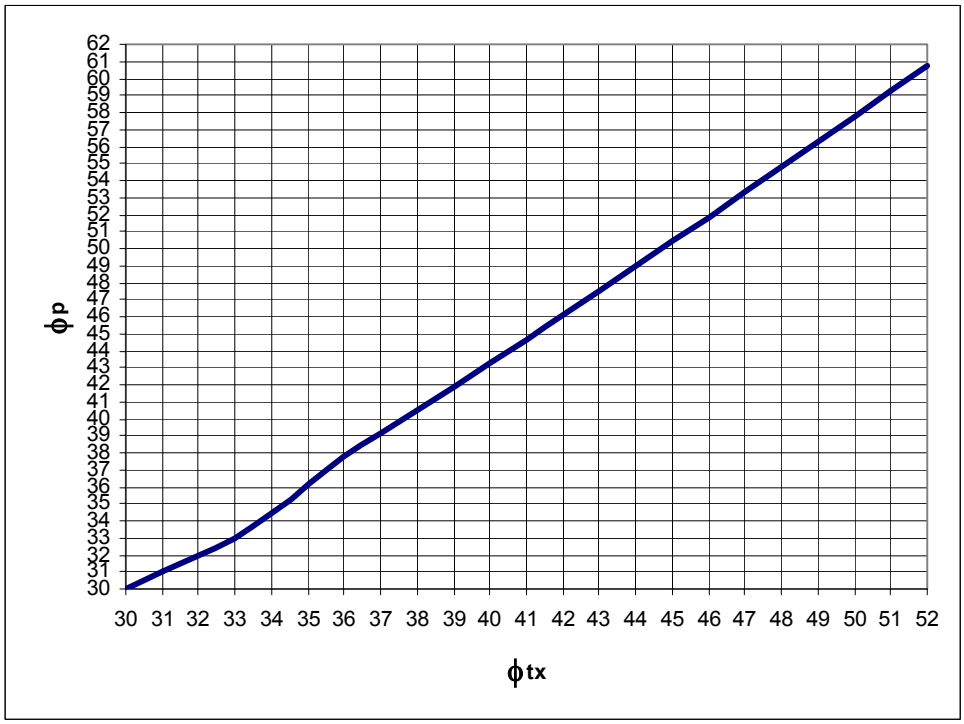

Figure 2.6: ϕ_p versus ϕ_{tx} (Bishop, 1966).

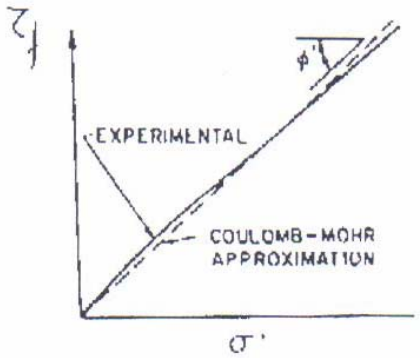

Figure 2.7: Mohr-Coulomb' stress at failure and failure envelope obtained from conventional drained triaxial compression test on sand.

2.3 Size effects in the ultimate bearing capacity formulae.

Tatsuoka *et al.* (1991) investigated experimentally and analytically the effects of the spread footing size in the bearing capacity. They found that size effects are caused by confining stress level effects on shear strength, progressive failure of foundation grounds and scale effects of footing width with respect to the particle size of ground materials. It should be noted that the scale effect cannot be detected in centrifuge loadings tests, and Ovesen (1979) commented that the scale effect is emphasized only in small scaled footings whose footings width B is less than 30 times the grain size (d_{50}) of foundation ground material. Tatsuoka *et al.* (1991) succeeded in simulating the size dependent behaviors of spread footings by means of an advanced FEM. However, simplified methods which incorporate the conventional bearing capacity formula are needed for practical design purposes.

There are simplified methods taking the stress level effects into account, in which the stress level effect is regarded as a main cause of the size effects. Meyerhof (1951) and De Beer (1970) proposed that the angle of internal friction ϕ to be applied to the bearing capacity formula, must be selected in accordance with the stress level beneath the footing. Meyerhof (1950) suggested that the mean normal stress on the failure planes σ_o is about a tenth of ultimate bearing capacity q_u, and De Beer (1970) presented the formula for averaged σ_o as:

$$\sigma_o = \frac{q_u + 3\gamma D_f}{4}(1 - \sin\phi) \qquad (2.12)$$

Though this type of methods seems to be promising for practical design, it is applicable only to cohesionless soils and not to materials with cohesion, such as cemented sand and gravel, because internal friction is determined from secant line to curved failure envelope, and the term for cohesion c in the bearing capacity formula is neglected in their methods. Also an iterative process is needed for determining the angle of internal friction ϕ corresponding to the stress range of interest, because the stress level is given as a function of

ultimate bearing capacity q_u. The logarithmic relationship of ϕ for Maipo sand, used in the present research, with confining stress σ_3 at different relative densities is shown in figure 2.8.

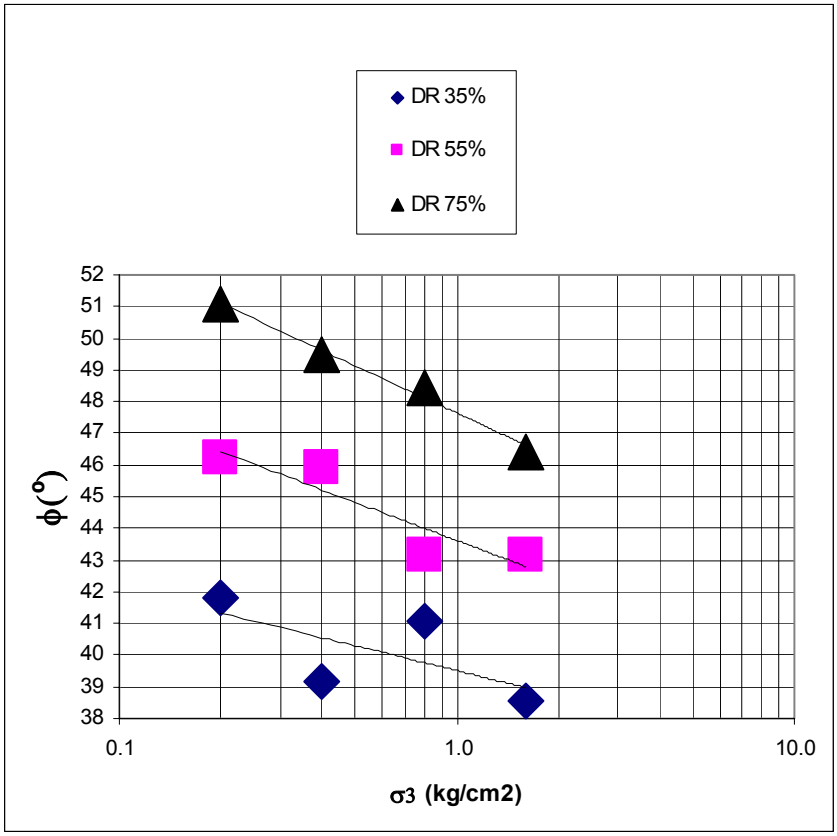

Figure 2.8: Semi-logarithmic relationship between ϕ determined from triaxial tests and the confining pressure σ_3.

III. FORMING UNIFORM BEDS OF SAND FOR MODEL FOUNDATION TESTS IN THE LABORATORY.

3.1 Introduction.

In natural deposits of sand, variations in porosity, void ratio or relative density, occur between different levels and from point to point horizontally, often in random way within the space of centimetres. When experiments with small model foundations are to be made, the scale of work demands a greater uniformity of porosity throughout the bed than can usually be found in nature and need to reproduce the same experimental conditions at will, over and over again, generally precludes making use of natural deposits. The experimenter, therefore, requires a method of forming artificial beds of sand that are homogeneous and reproducible over wide range of porosities.

The apparatus described was developed for preparing beds of sand in cubical containers 1.0m x 1.0m sides and up to about 0.65m deep for tests on model shallow foundations. Only one type of sand has been used in the apparatus. The distribution of the sand density was the most important aspect, since a complete homogeneity was needed to carry out the ultimate bearing capacity tests.

The effects of the method of preparing test specimens in the static stress-strain behaviour on sand specimens, which had different angularity, was studied by Oda in 1972 (Mulilis *et al*.,1975) on cyclic drained triaxial strength testing using two distinct method of preparing: *tapping*, the sand inside the mold is densified through blows external to the mold, and *plunging*, where the blows are applied by layers inside the mold with a hammer. From the obtained results Oda could conclude that the *tapping* method led to strength , tangent modulus and dilatancies significantly greater than the method of *plunging*.

Mahmood in 1973 (Mulilis et al.,1975) studied the compressibility and structure characteristics of Monterey Nº0 sand specimens through two methods: *pluviation*, where the sand is poured through the air inside the mold, and *vibration*, the specimen was

compacted over the top edge of the mold. The results obtained with the dense sand specimens indicated that although the *pluviation* and *vibration* produced specimens which particles had random orientation, the specimens formed by *pluviation* were more compressible and shown greater lateral deformations than the specimens formed by vibration.

Ladd (1974) carried out cyclic triaxial tests under controlled stress on saturated specimens of three prepared different sands by means of two methods: *dry vibration*, vertical vibration applied to the specimen, and *wet tamping*, where each layer was compacted by hand tamping with a 25mm diam compaction foot instead of the vibration tool. The initial water content of the compacted material is approx 9% instead of zero. Based on the data presented, Ladd concluded that the liquefaction behaviour of reconstituted specimens of sand tested in triaxial equipment may be significantly affected by the method of specimen preparation. The potential of liquefaction of the specimens prepared by *dry vibration* was until 100% superior to the specimens of equal density prepared by *wet tamping*.

Another technique also applied in the preparation of specimens to cyclic triaxial tests was the *undercompaction* (Ladd, 1974 and 1978; Mulilis et al.,1975; Tatsuoka et al.,1986). This approach was selected since it is generally recognized, especially for loose to medium dense sands, that when a typical sand is compacted in layers, the compaction of each succeeding layer can further densify the sand below it. The method uses this fact to achieve uniform specimens by applying the concept of *undercompaction*. In this case, each layer is typically compacted to a lower density than the final desired value by a predetermined amount which is defined as percent *undercompaction*. In the preliminary investigations realized by Mulilis et al. (1975) it was determined the optimum value of percent *undercompaction* to produce an uniform density specimen throughout their length, and to compare with the distribution of specimens prepared without this technique.

The density distribution inside the specimen prepared by four different methods of compaction, i.e., pluviation, horizontal vibration with high and low frequency in layers

with 12% of undercompaction and horizontal vibrations of high frequency in a layer of 7", gave the values of relative density for each layer shown in the table 3.1 (Mulilis et al., 1975).

Table 3.1: Relative densities (%) distribution in specimens of 2.8" diameter.
(Mulilis et al., 1975).

Layers measured	*Pluviation*	horizontal vibration of low frequency (7 layers of 1")	horizontal vibration of high frequency (7 layers of 1")	horizontal vibration of high frequency (1 layers of 7")
1st (2")	55	49	50	64
2nd (2")	56	51	49	46
3rd (2")	53	50	46	37
4th (1")	55	52	55	48
mean	55	50	49	49
maximal difference	3	3	9	27

From the results shown in the table 3.1, it can be noticed that the compactation by *pluviation* and *horizontal vibration of low frequency* produced the most uniform specimens, instead the compaction by horizontal vibration of high frequency on 7 layers of 1" produced less uniformity. The compaction of high frequency in a layer of 18cm yielded a total heterogeneous specimen.

Additionally, Mulilis et al. (1975) took radiographies to the specimens sections prepared by three different methods of compaction: pluviation through the air, external horizontal vibrations with high frequency after compacted each layer and the tamping method. Owing to less x-ray pass through dense sections, this sections appear smoother in a negative of a film (or darker in a positive film or photo) and vice-versa for loose sections. Although the reproduction quality isn't good, the differences in the distribution of densities can be too observed (see figure 3.1). The conclusions are:

a) The specimens formed by raining present thin layers of loose and dense material continuously alternate.

b) The specimens compacted by horizontal vibration are composed of relatively uniform density layers, each one separated by a thin and high density lens. These lenses are formed due to the surcharge that is lying on the surface of each layer when those are densifying.

c) The tamped compacted specimen presented the less uniformity material. Each layer varies from a loose condition to a dense condition inside the each layer.

According to these findings, it can be concluded that the specimens formed by the pluviation or raining method present a mayor homogeneity. It can also be verified from the simple visual inspection of the figure 3.1.

All of this preparation techniques are referred to the specimens preparation for triaxial tests, direct shear or torsional cyclic shear tests, corresponding to small size specimens. In the following the filling up of a container will be analysed, aspect of the special relevance to this investigation.

3.2 Design of an apparatus to place sand using the pluviation method over a large cubic container

The reconstitution of granular soil models is the first problem to consider in a experimental analysis. Many researchers have carried out this investigation as part of laboratory testing programs (Walker and Whitaker, 1967; De Beer, 1970; Ko and Davidson, 1973; De Alba et al., 1975; Krajewski, 1986; Passalacqua, 1991; Gottardi and Butterfield, 1993; Gottardi et al., 1994; Perau, 1997; Sawicki et al.,1998; Laue, 1998; Lee et al., 1998, etc.).

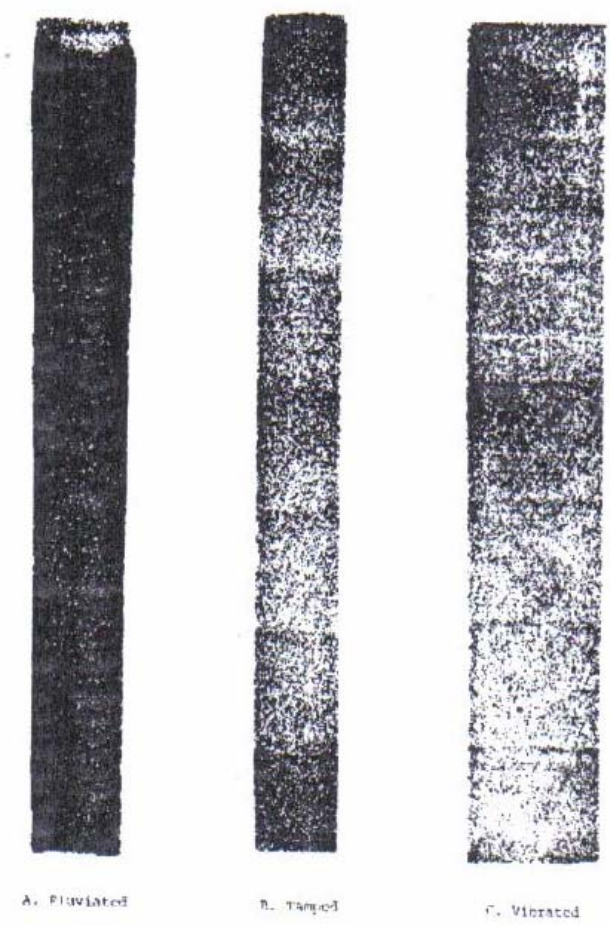

Figure 3.1: Radiographies of sand specimens sections prepared by different compaction methods (Mulilis et al.,1975).

Walker and Whitaker (1967) performed an interesting investigation that led to a design of an apparatus which deposits sand in circular containers 90cm diameter and up to about 120cm deep. The apparatus was developed for preparing uniform beds of sand for a series of model pile experiments. The same idea was incorporated by De Alba *et al.* (1975) as well as by Gottardi *et al.* (1994) and many others. Circular in plan containers were chosen because of the greater rigidity of their walls under internal lateral pressure than the walls of rectangular containers, and because the tests proposed had axial symmetry (Walker, 1964).

The inside chamber dimensions were 1.0m x 1.0m wide by 0.65m deep. The chamber was filled with a uniform and fine sand. The source of this sand is the Maipo river

which properties it will be describe farther on. The sand placement it was carry out through the pluviation or raining technique. This technique is not new, along the years many researchers have employed it to test scale models over cohesionless soils. For example, it can be mentioned to Brinch Hansen (1970); De Beer (1970); Walker y Whitaker (1967); Gottardi (1994, 1999) and Selig and McKee (1961).

The sand spreader assembly (SSA) was designed in order to the mechanism for applying vertical loads to the model foundations (the plate), including the reaction frame fitted to the laboratory slab, could be placed over and around the chamber without touching or affecting at all, thus avoiding any risk of altering the initial state of compaction of the sand.

3.3 Controlled placement of sand.

Walker y Whitaker (1967) analysed different factors that influence the controlled placement by raining of sand. Among such factors it can be pointed out the intensity of the rain , i.e. the weight deposited per unit area in unit time, and the drop height of the particles. For a given height, an increase in the intensity increased the porosity, while for a given intensity, an increase in the drop height decreased the porosity. This increase is true until a certain value of drop height, it appears from the test results that increase in impact energy beyond a certain maximum magnitude may do little. Although for a given sand, the intensity of placement and drop height control the resulting relative density sufficiently accurate for most experimental purposes, there is evidence that particle sphericity are also significant when comparisons are made between different kind of sands.

Mulilis *et al.* (1975) concluded from their tests with Monterey Nº0 sand that to obtain specimens of 7” height and 2.8” diameter, with relative densities of 50%, 70% and 85% by the method of raining, it was necessary to use a pipe like the showed one in the figure 3.2, with openings of 6.9, 5.1 and 3.8mm, respectively, with a drop height of 50cm. In this manner it confirms that the use of greater diameters produce the more intense rain of

sand and the lower dry densities. After Mulilis *et al.* (1975), the openings diameters is more important than the drop height, in the range investigated by them, varying from 15 to 50cm.

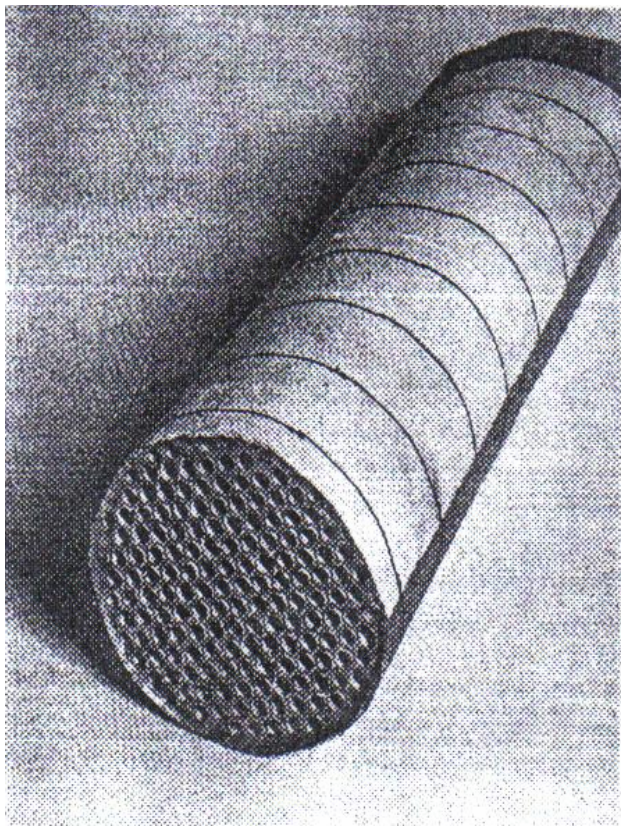

Figure 3.2: Cylindrical pipe for the placement of sand used by Mulilis *et al.* (1975).

De Alba et al. (1975) point out that from their own experimental results with the sand by pluviation filling in a chamber of large size, they could verify too that the drop height would have a low incidence in the relative density obtained.

In the early stage of the present investigation several possibilities of mechanism were analysed to allow form a homogeneous specimen of sand. One of this was to apply a motorized system by pouring the sand following the procedure used by Walker and Witaker (1967), De Beer (1970) and De Alba *et al.* (1975) among others. However, this procedure was discarded due to their complexity, practical limitations and due to also their high cost.

The sand spreader assembly (SSA) designed and built in the Geotechnical and Structural Engineering Department, with the collaboration of the Mechanical and Metallurgical Engineering Department belonging to the Pontificia Universidad Católica de Chile, allows to use perforated plates that can be removed and therefore to change the perforations diameters or the deposition intensity. On another hand the SSA allows to vary also the drop height of sand. Figures 3.3 and 3.4 depict different views of the SSA, showing their principal parts.

In the domestic market there are different types of perforated plates as shown in figure 3.5. It was only used two types of this plates. One 2mm thickness plate with 2mm diameter openings, spaced 3.5mm (between their centres) (R2 T3.5), and another 3mm thickness plate with 3mm diameter openings, spaced 5mm (R3 T5). The first one has a perforation effective area of 23% and the second have a perforation effective area of 32.6%. Neither of the two plates used shown some flexural deformation problem during the sand pouring because they were clamped all along their perimeter.

In the beginning both perforated plates were used to choose the appropriate settings on the sand release opening width, i.e., the 2mm and 3mm, however, the relative density obtained by the above last plate, lies under the 53% value for ours conditions. In accordance with Vesic' studies (1973) (see figures 3.6 and 3.7), the mentioned range of densities corresponds to a footing on loose sand and in local shear zone. This was corroborated for the graphical results of the tests presented here. Then this hypothesis could be demonstrated. For that reason it was not thought recommendable to analyse such tests under the classical ultimate bearing capacity theory.

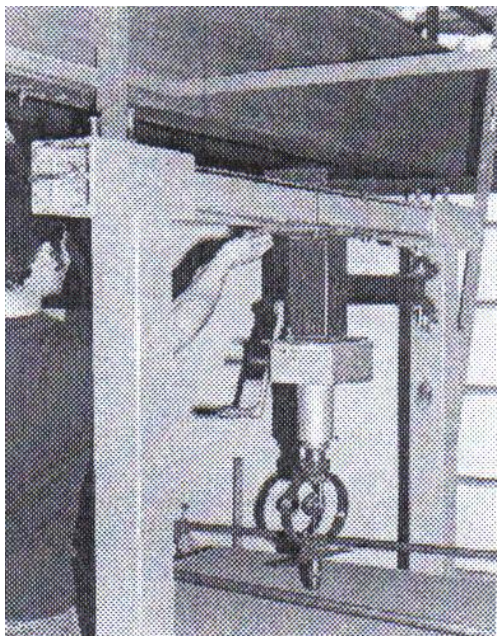

Figure 3.3: View showing the set up of the upper beam of the reaction frame and installation of the rotating arm with the hydraulic jack, load ring and steel load application piece.

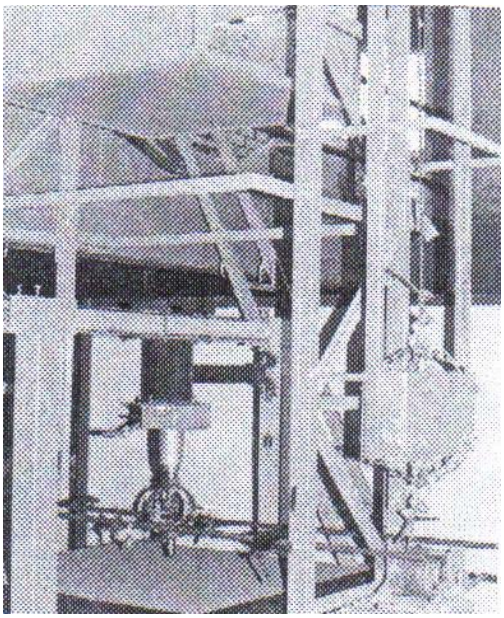

Figure 3.4: Sand Spreader Assembly (SSA) photograph: Reaction frame, hydraulic jack, load lecture ring and LVDT.

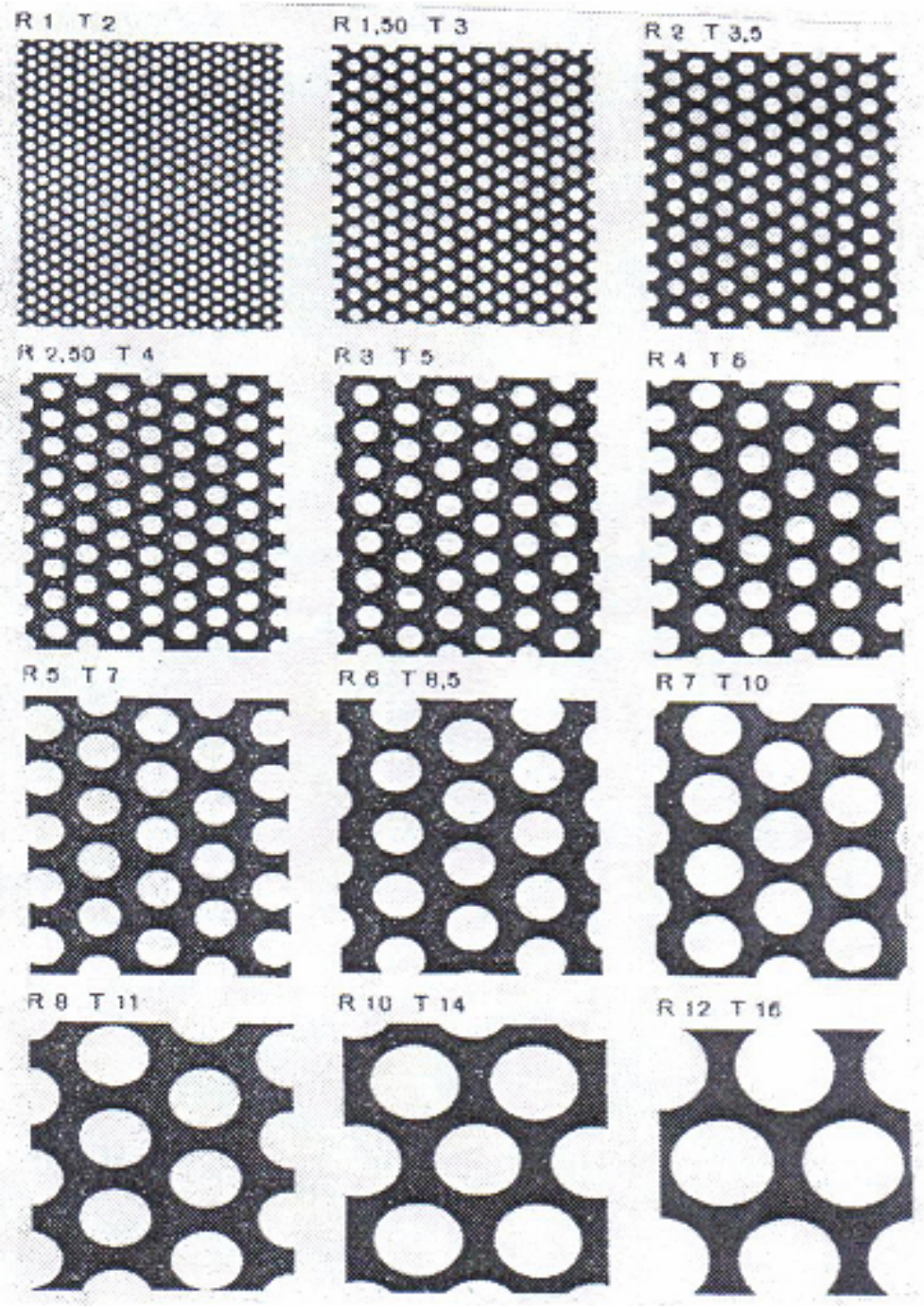

Figure 3.5: Detail of the perforated plates available in the domestic market (Brainbauer).

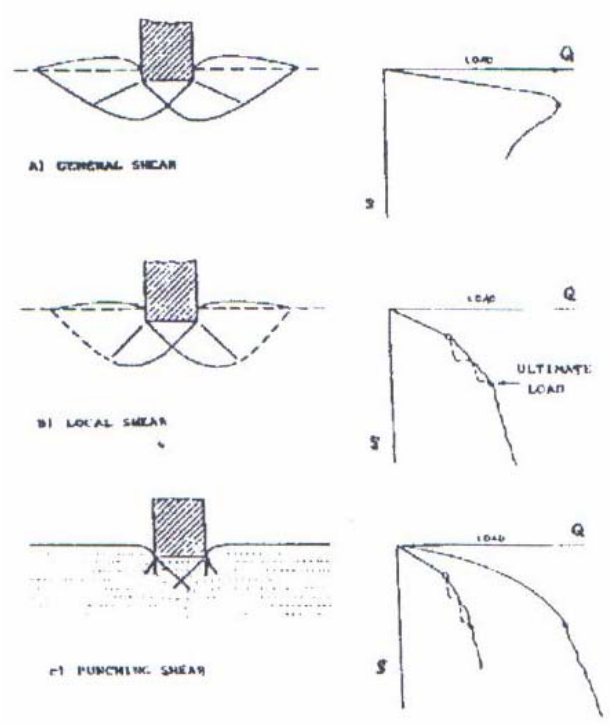

Figure 3.6: Modes of bearing capacity failure (Vesic, 1973).

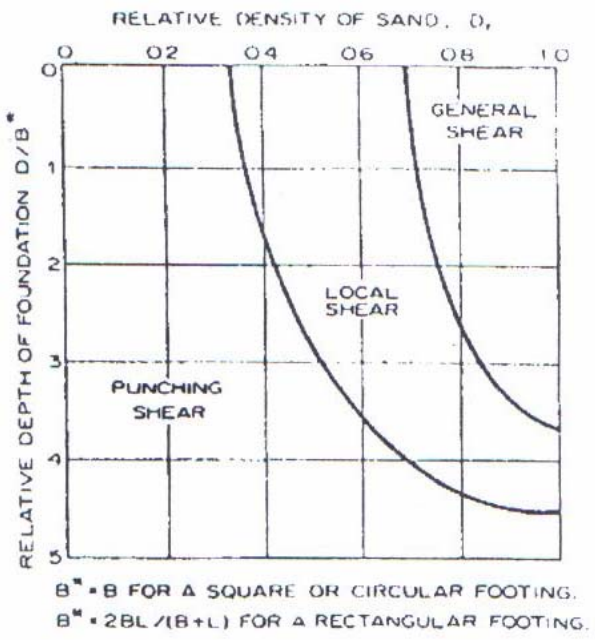

Figure 3.7: Modes of failure of footings in Chattahoochee sand (Vesic,1973).

As a consequence of the above only the 2mm openings plate were subsequently used, allowing to obtain relative densities in the range of 53 to 70%.

The figure 3.8 shows the drawings of the SSA in AUTOCAD format. It can be noticed the detail of the drop height control system over the chamber. The system works with a trolley attached to a railed frame and is driven back and forth by hand with a winch over the container or chamber while the sand is sprinkled in. The rise rate of the trolley must be slow, in order to avoid any undesirable potential energy influences caused by continuous variation of sand volume, the advance of the trolley was of 1cm per two turns of the winch. A feeder is set at the top of the assembly providing a continuous flow of sand through a single hose of 4.5cm inside diameter. The sand flows through the hose and is discharged onto a diffuser plate which breaks the stream of sand and causes the sand to be evenly distributed on the specimen surface (see figures 3.9, 3.10 and 3.11). The profile of the specimen surface was controlled by changing the direction of the flexible hose, and lift density was controlled by the drop height and intensity of raining. Intensity of raining refers to the rate of sand discharge, and was regulated by inserting plates with various hole sizes, between the reservoir or chamber and the flexible tube. The maximum drop height of the SSA is approximately 1.5m. Fortunately this restriction produces no effect in the densities required in the tests due to the calibration of the SSA, described below, showing that no greater densities are obtained over 80cm of drop height.

3.4 SSA CALIBRATION

Tables 3.2 and 3.3 give the results obtained with the SSA for the Maipo sand here tested. In fact, the values correspond to the drop height H and the relative density DR.

The results obtained can be shown by plotting DR against the drop height H and against the opening width.

The rate of reservoir filling was 1.1cm/min within the range of drop height of 50 to 70cm for the 2mm diameter openings plate.

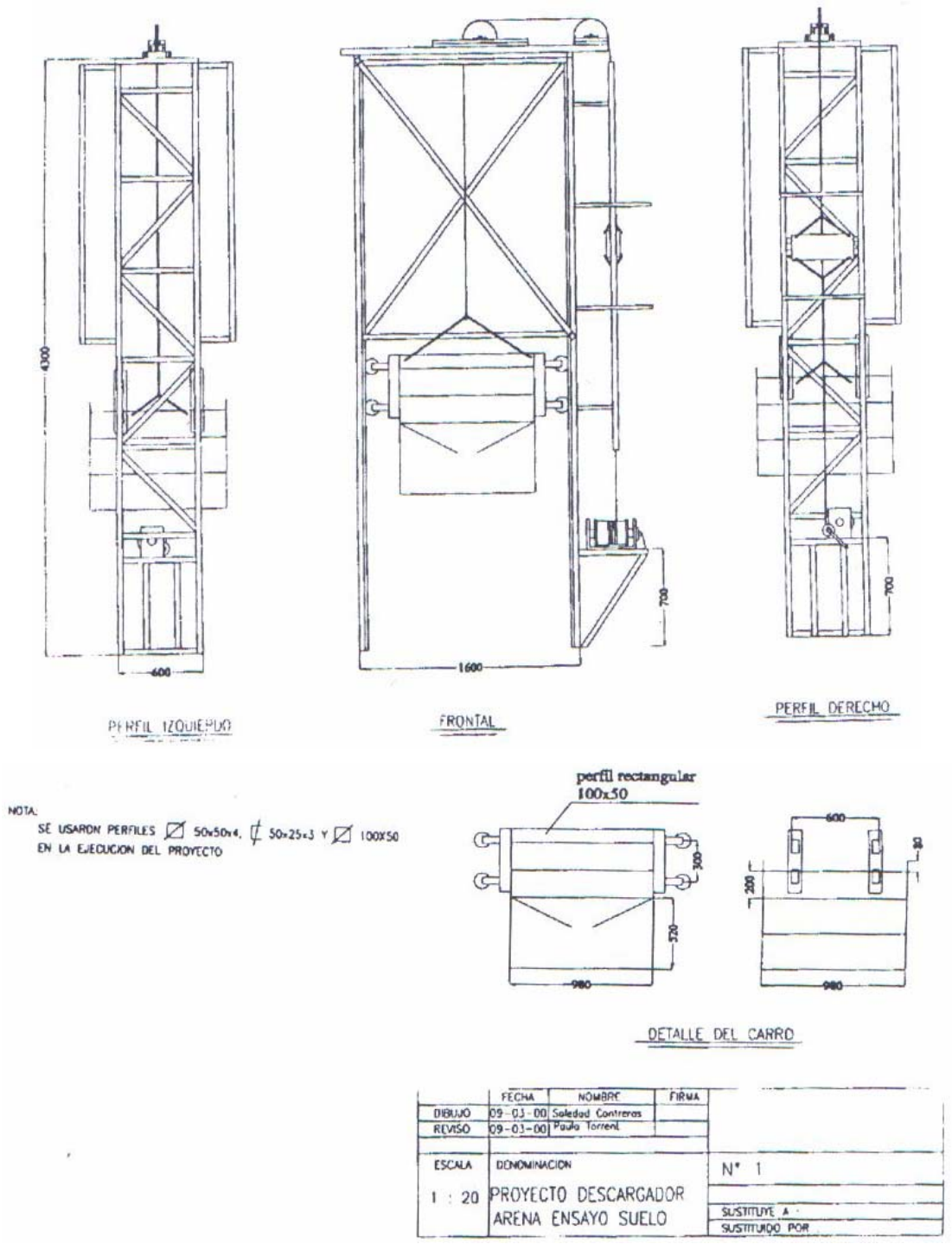

Figure 3.8: Sand spreader assembly SSA.

Table 3.2: Equipment calibration for 2mm openings.

DR(%)	H (cm)
59	100
63	80
61	80
58	70
70	65
65	60
60	60
53	50
50	10

Table 3.3: Equipment calibration for 3mm openings.

DR(%)	H (cm)
50	120
52	100
52	80
45	60
51	50
52	50
48	40
43	20
30	10

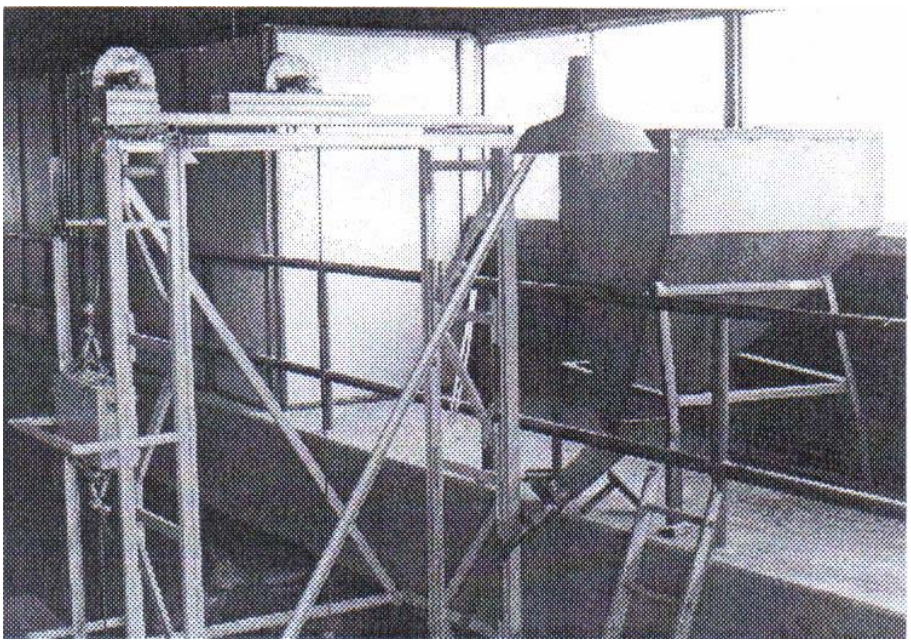

Figure 3.9: Equipment SSA: Feeder box of sand, exit funnel and flexible hose.

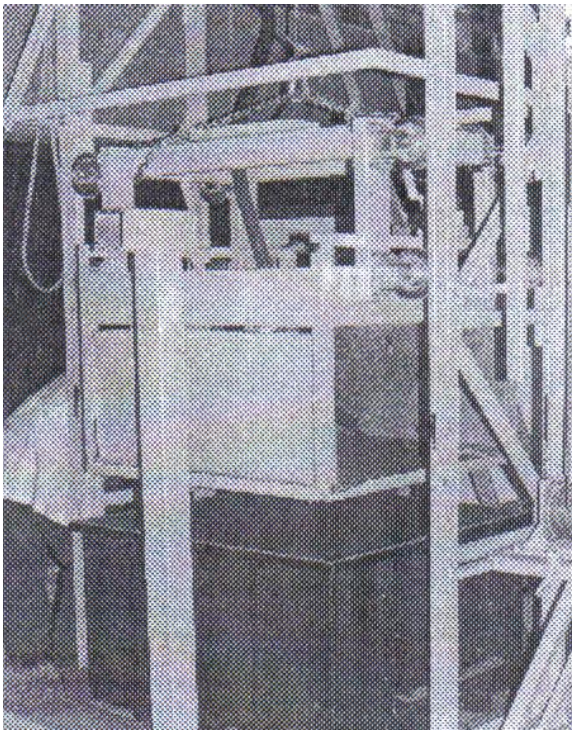

Figure 3.10: Pouring of sand with the flexible hose over the perforated plate.

Figure 3.11: Nearer view of the sand pouring over the perforated plate.

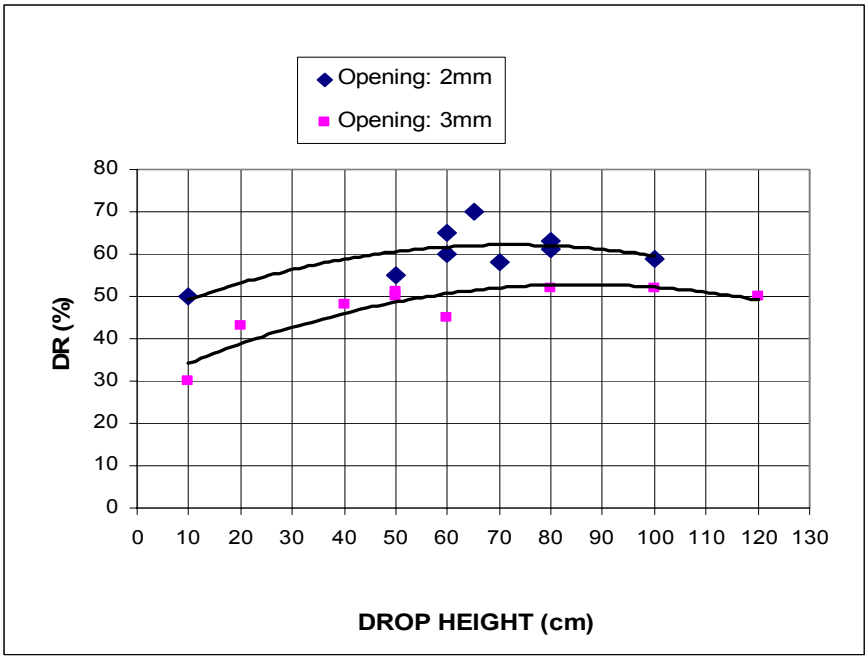

Figure 3.12: Calibration graph for Maipo sand for the pluviation method.

3.4.1 Direct measurements of relative density.

The relative density determination procedures of the specimens prepared by the sand pluviation method at the laboratory consisted in: measure the chamber volume filled for the deposited sand and weigh such sand volume, including the chamber weight by means of a digital dynamometer DYNA LINK 2500kg of capacity and 1kg of sensibility. The figure 3.13 shows the weight system used. It was used the same reaction frame. Once fulfilled the above procedure, the mean density of the dry sand γ_d is computed and then the relative density is determined by means of the formula:

$$DR = \frac{\gamma_{dmax}}{\gamma_d} \cdot \frac{\gamma_d - \gamma_{dmin}}{\gamma_{dmax} - \gamma_{dmin}} \cdot 100(\%) \qquad (3.1)$$

The values of γ_{dmin} and γ_{dmax} are presented in the section of index properties of the Maipo sand.

3.4.2 Variability of relative density.

Variations of relative density from point to point within the container can be caused by many factors, some of which are inherent in this particular method of placement, while others are presented in any technique involving significant quantity of sand. When the rain of sand has traversed the perforated plate and entered inside the container, the air currents it causes, flowing forward from the rain towards the wall of the container, are reflected back to the central part of the sand rain. The resulting disturbance decreases the intensity of deposition, thus decreasing the relative density. As a corrective measure, the operator must pour the sand over the perforated plate following always a slow movement, keeping an horizontal and even level of sand inside the container.

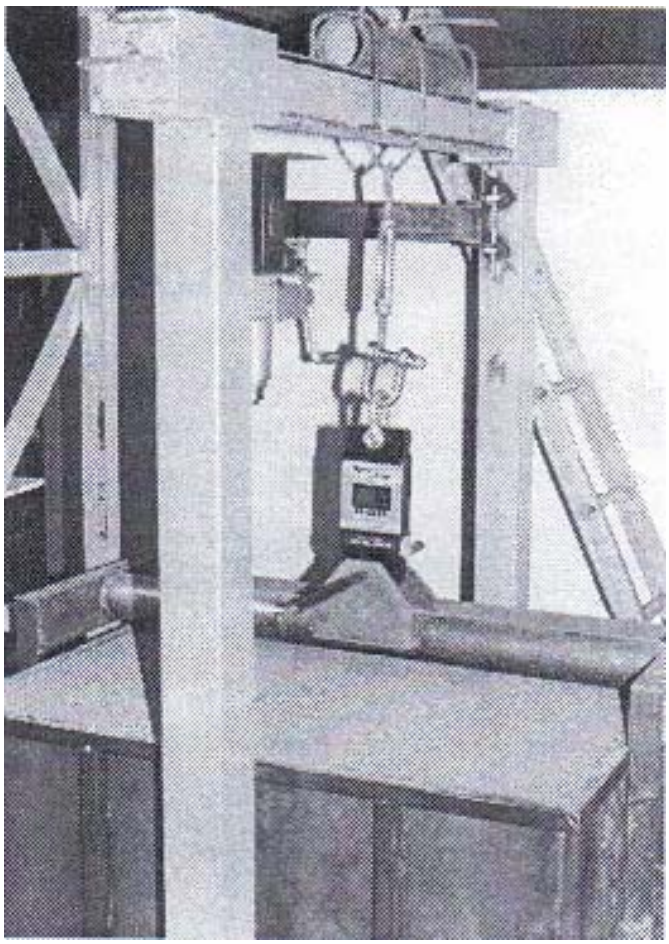

Figure 3.13: Weight system of the container filled with the sand after the bearing capacity test was carried out. Dynamometer used DYNA LINK.

3.5 Application system of load.

3.5.1 Structural and mechanical conditions of the equipment used.

The vertical load plate tests was performed in the interior of the Geotechnical Engineering Laboratory in order to achieve and keep stable environmental conditions (temperature, air currents, moisture, etc.).

Figures 3.3 and 3.4 show the reaction frame used in the testing. It can be noticed that the frame has two steel columns fitted at the floor of the laboratory room. A horizontal sliding steel beam rest above them, but restrained to displace in the vertical direction by means of two adjustment bolts. The frame capacity is about 1600kg due to the limited pulling out strength of the bolt anchored to the slab. Nevertheless, this capacity provided strength enough to all the tests performed.

All the analysis of bearing capacity presented are developed for static loading conditions. It assumed that footing load is increased gradually until failure at a loading rate slow enough so that no viscous or inertia effects are felt. The rate of application of the load was about 1mm/min. The control of the application of the load was carried out by means of two load rings Clockhouse Engineering for 400lb until 2000lb, regarding the need. The precision of the first is 0.125kg per division, and for the second 0.580kg per division.

To the application of the vertical load it was used a hydraulic jack used often in the in situ CBR test execution. This jack offered the possibility to work with controlled displacement rate.

The load was applied direct to the test plate (the model prototype footing) by means of a steel load application piece with a semi spherical peak, which introduced inside of a semi spherical cavity also machined over the superior face load plate to assure the verticality of the load and avoid the presence of bending moments that might be generate eccentricities.

The settlement of the test plate was measured with high sensibility LVDT transducers, placed in the way shown in the figure 3.14. The LVDT was connected to a power source with the aim to acquire the necessary voltage. The portable data recording equipment TDS-302, by Tokyo Sokki Kenkyujo Co., Ltd., allowed to measure the voltage variation, which, as it is well known, is in correlation with the settlements of the load plate (see figures 3.14 and 3.15).

3.6 Sand for testing

3.6.1 Index properties

The sand used is a sediment of the Maipo river deposited in the Vizcachas zone, near of Santiago. This sand was prepared with the purpose to produce a uniform sand without fines. The figure 3.16 shows the classification and grain size distribution; d_{50} = 0.32mm, uniformity coefficient C_u = 1.9, curvature coefficient C_c = 1.0 and specific gravity of G_s = 2.70gr/cm^3. In the figure are included too the grain size distributions of sand used in other analogous researchs (Ko and Davidson, 1973; Walker and Whitaker, 1967, Ladd, 1978; De Alba et al.,1975; Mulilis et al., 1975, Tatsuoka et al., 1986, De Beer, 1970, Gottardi et al., 1999, and Bieganousky and Marcuson, 1976).

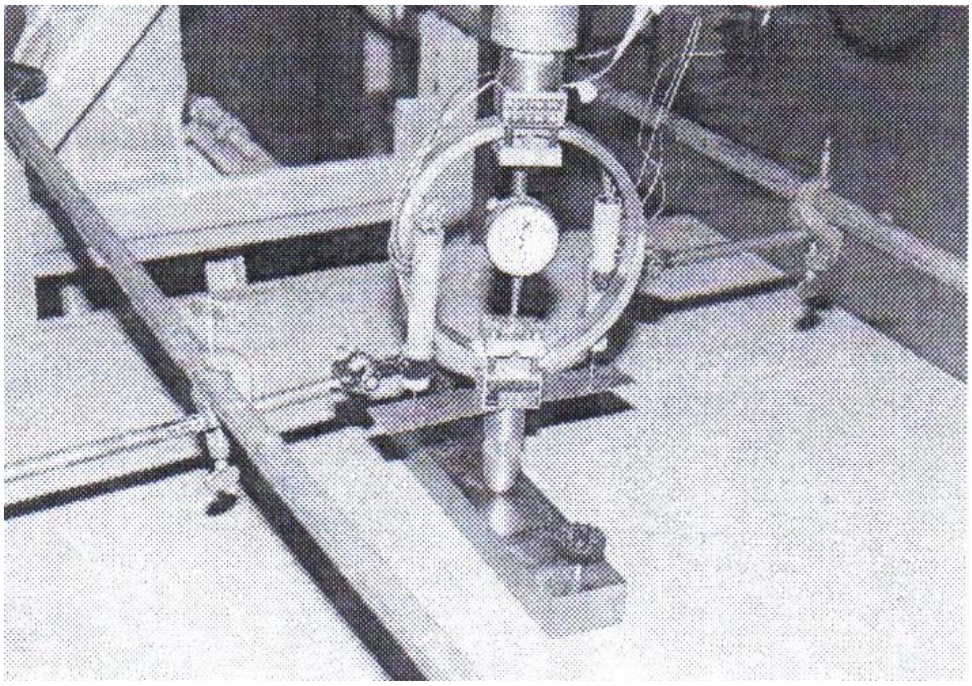

Figure 3.14: Transducers LVDT 1000, and load ring Clockhouse Engineering.

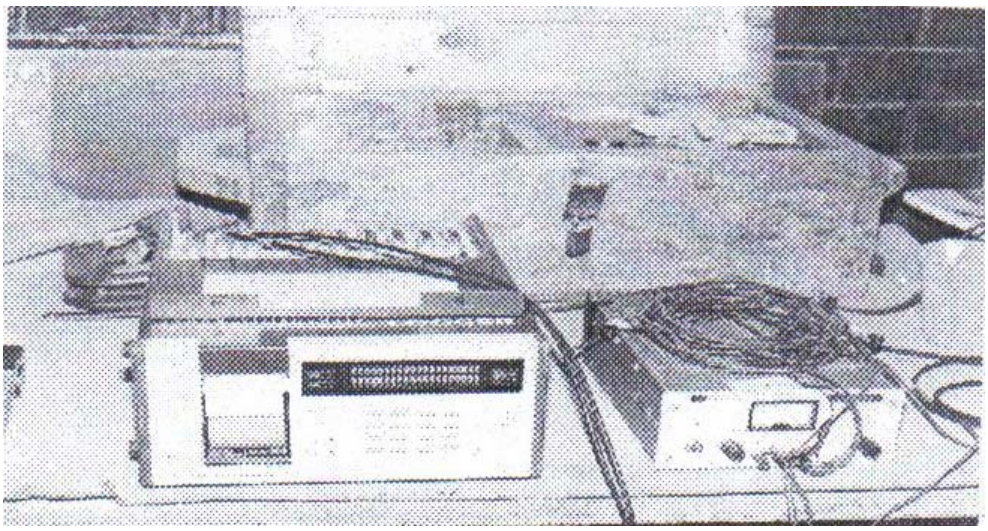

Figure 3.15: View of the portable data recording equipment TDS-302, by Tokyo Sokki Kenkyujo Co., Ltd. and the power source used.

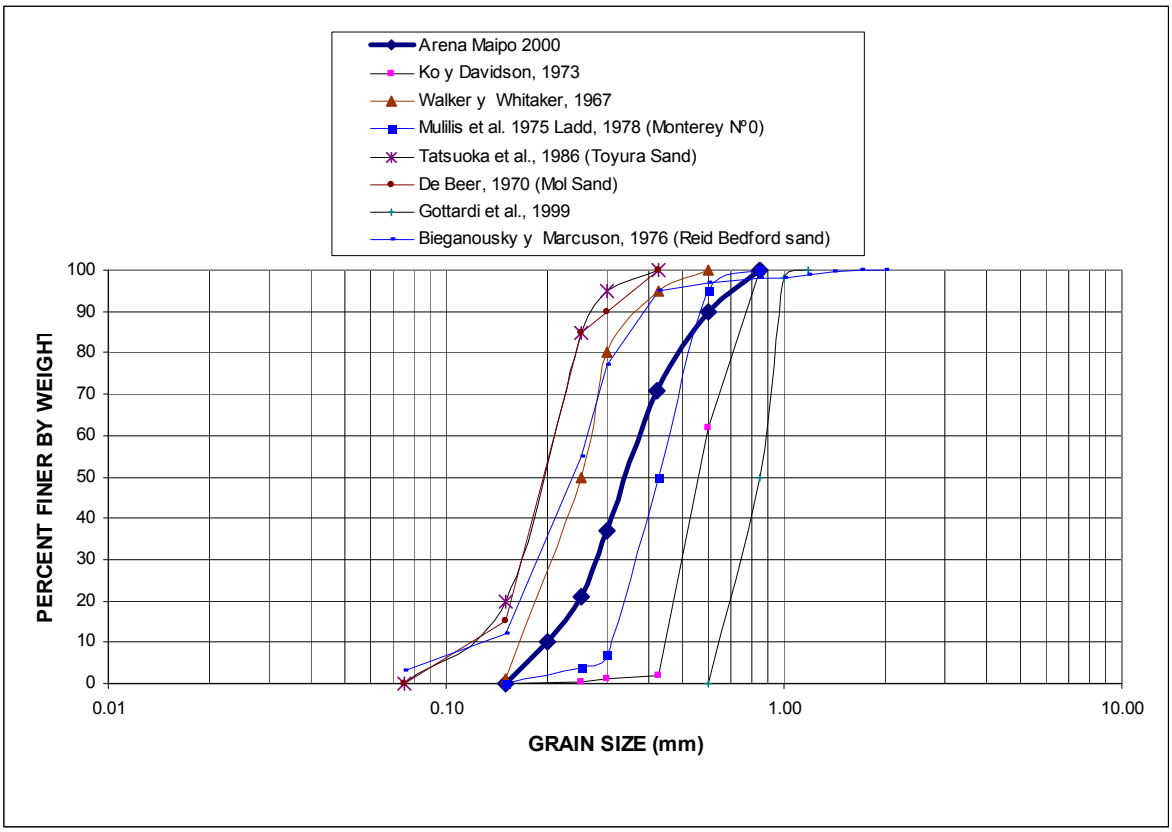

Figure 3.16: Grain size distributions of used sand.

It could be observed that all curves present a uniform granulometry to avoid segregation problems. Also, in our case the fraction under the mesh ASTM Nº100 (0.125mm) was eliminated to prevent the undesirable effect of the fines. With a continued use of the same sand, some change is unavoidable because of the dust released to the atmosphere during the placement and also because of the crushing of sand grains during handling and testing. Although no difference in the grading could be detected during the series of tests by normal sieving methods and the model footing tests detected no slight change for this reason.

The reported values for dry densities, minimum and maximum (1.291 y 1.660T/m^3) have been determined by minimum and maximum void ratio measurements from laboratory samples at the densest and loosest states according to the standards ASTM D 4254-91 and ASTM D 4253-93. The table 3.4 gives the values of relative density DR, dry density γ_d, void ratio *e* and the porosity *n* of the sand tested. Figure 3.17 is a plot of dry density γ_d versus DR and porosity.

3.6.2 Mineralogy

Through the micro analytical characterization of the material by means of scanning electronic equipment a quantitative and qualitative characterization of the material could be made. This material is in average 70% siliceous oxide SiO_2. Also, there is a presence of aluminium oxide Al_2O_3, with an average content of 16%. The sand grains characterize by to present few significant concentrations of alkaline ions (Na and K) and alkaline-terreous (Ca and Mg) and the existence of the kind of mineral feldspar. It was observed in some sand grains the presence of small ferrous inclusions (magnetite Fe_2O_3). A scanning microscope photograph of the sand soil is shown in figures 3.18 and 3.19.

Table 3.4: Dry density versus relative density.

DR(%)	γd (T/m^3)	e	n (%)	DR(%)	γd (t/m3)	e	n (%)
γd max =	1.660	(T/m3)		γd min =	1.291	(T/m3)	
0	1.291	1.091	52.2	51	1.456	0.854	46.1
1	1.294	1.087	52.1	52	1.460	0.850	45.9
2	1.297	1.082	52.0	53	1.463	0.845	45.8
3	1.300	1.077	51.9	54	1.467	0.840	45.7
4	1.303	1.073	51.8	55	1.471	0.836	45.5
5	1.306	1.068	51.6	56	1.475	0.831	45.4
6	1.308	1.064	51.5	57	1.478	0.826	45.2
7	1.311	1.059	51.4	58	1.482	0.822	45.1
8	1.314	1.054	51.3	59	1.486	0.817	45.0
9	1.317	1.050	51.2	60	1.490	0.812	44.8
10	1.320	1.045	51.1	61	1.494	0.808	44.7
11	1.323	1.040	51.0	62	1.497	0.803	44.5
12	1.326	1.036	50.9	63	1.501	0.799	44.4
13	1.329	1.031	50.8	64	1.505	0.794	44.3
14	1.332	1.026	50.6	65	1.509	0.789	44.1
15	1.336	1.022	50.5	66	1.513	0.785	44.0
16	1.339	1.017	50.4	67	1.517	0.780	43.8
17	1.342	1.012	50.3	68	1.521	0.775	43.7
18	1.345	1.008	50.2	69	1.525	0.771	43.5
19	1.348	1.003	50.1	70	1.529	0.766	43.4
20	1.351	0.998	50.0	71	1.533	0.761	43.2
21	1.354	0.994	49.8	72	1.537	0.757	43.1
22	1.357	0.989	49.7	73	1.541	0.752	42.9
23	1.361	0.984	49.6	74	1.545	0.747	42.8
24	1.364	0.980	49.5	75	1.549	0.743	42.6
25	1.367	0.975	49.4	76	1.553	0.738	42.5
26	1.370	0.971	49.3	77	1.558	0.733	42.3
27	1.373	0.966	49.1	78	1.562	0.729	42.2
28	1.377	0.961	49.0	79	1.566	0.724	42.0
29	1.380	0.957	48.9	80	1.570	0.719	41.8
30	1.383	0.952	48.8	81	1.574	0.715	41.7
31	1.387	0.947	48.6	82	1.579	0.710	41.5
32	1.390	0.943	48.5	83	1.583	0.706	41.4
33	1.393	0.938	48.4	84	1.587	0.701	41.2
34	1.397	0.933	48.3	85	1.592	0.696	41.0
35	1.400	0.929	48.2	86	1.596	0.692	40.9
36	1.403	0.924	48.0	87	1.601	0.687	40.7
37	1.407	0.919	47.9	88	1.605	0.682	40.6
38	1.410	0.915	47.8	89	1.609	0.678	40.4
39	1.414	0.910	47.6	90	1.614	0.673	40.2
40	1.417	0.905	47.5	91	1.618	0.668	40.1
41	1.420	0.901	47.4	92	1.623	0.664	39.9
42	1.424	0.896	47.3	93	1.627	0.659	39.7
43	1.427	0.891	47.1	94	1.632	0.654	39.6
44	1.431	0.887	47.0	95	1.637	0.650	39.4

45	1.434	0.882	46.9
46	1.438	0.878	46.7
47	1.442	0.873	46.6
48	1.445	0.868	46.5
49	1.449	0.864	46.3
50	1.452	0.859	46.2

96	1.641	0.645	39.2
97	1.646	0.640	39.0
98	1.651	0.636	38.9
99	1.655	0.631	38.7
100	1.660	0.627	38.5

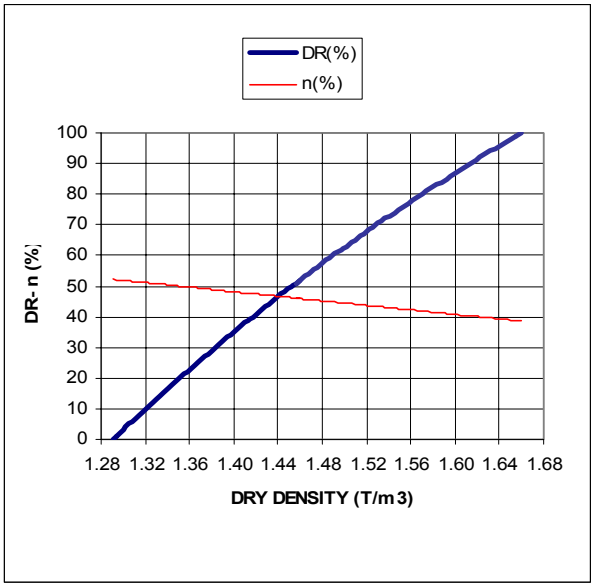

Figure 3.17: Relative density (porosity) versus dry density.

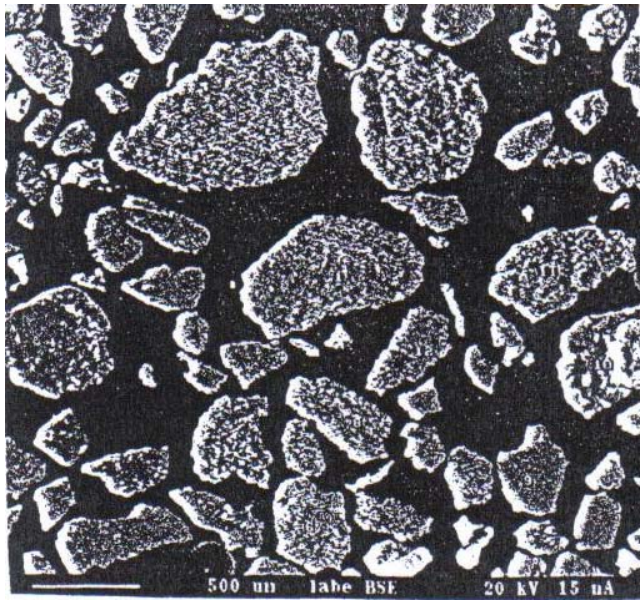

Figure 3.18: Scanning electron microscope photograph of sand soil particles tested (IDIEM, 2000).

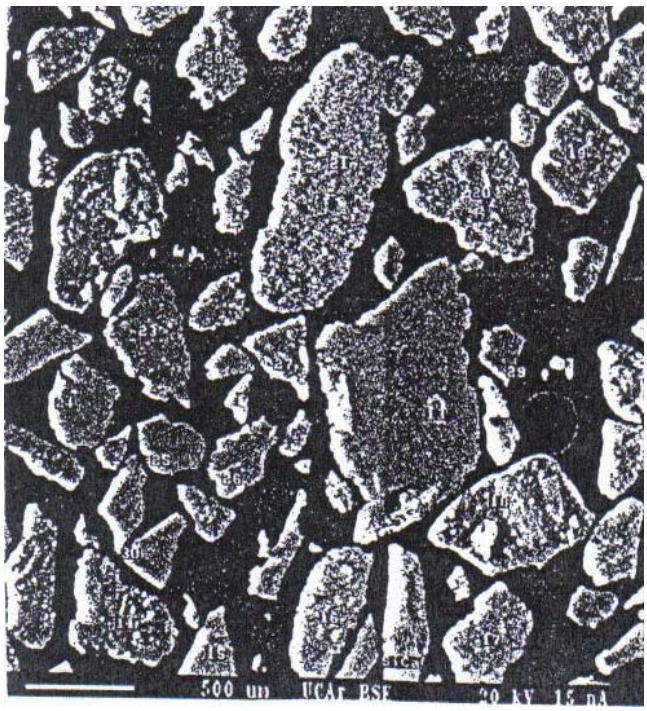

Figure 3.19: Scanning electron microscope photograph of sand soil particles tested (IDIEM, 2000).

3.6.3 Geomechanical properties.

Table 3.5 summarizes the internal friction angle values obtained in triaxial tests. These values have been plotted in a p-q graph for each relative density tested, and the angle of internal friction was determined applying the formula:

$$\phi = \sin^{-1}(\tan\alpha) \qquad \text{where} \qquad \tan\alpha = q/p \qquad (3.2)$$

In figures 3.20, 3.21 and 3.22 a curve has been fitted to the experimental data. These curves correspond to the better lineal fit of the points (p,q). Due to the low confining stresses level, with the purpose to reproduce the subsoil conditions underneath the shallow plate, the lineal fit was excellent. It can be assumed a lineal behaviour of the Mohr – Coulomb

envelope for low confining stresses. Figure 3.23 plots the values of ϕ versus relative density. The correlation coefficient for the lineal fit of the three point, was $R^2 = 0.9991$ expressed by the following equation:

$$\phi = 0.1984DR + 32.297 \qquad (3.3)$$

where, ϕ : angle of internal friction in sexagesimal degrees and DR : relative density in %.

This formula is similar to the proposed one by Meyerhof: ϕ = 0.15DR + 30, for sand with a fine content less than 5%.

Table 3.5: Triaxial tests results by the Maipo sand.

	DR = 35%		DR = 55%		DR = 75%	
σ3 (Kg/cm2)	ϕ (°)	σ1 at failure (Kg/cm2)	ϕ (°)	σ1 at failure (Kg/cm2)	ϕ (°)	σ1 at failure (Kg/cm2)
0.2	41.81	1.000	46.24	1.240	51.06	1.600
0.4	39.19	1.773	45.92	2.441	49.51	2.941
0.8	41.05	3.861	43.14	4.260	48.45	5.559
1.6	38.57	6.899	43.14	8.520	46.44	10.022

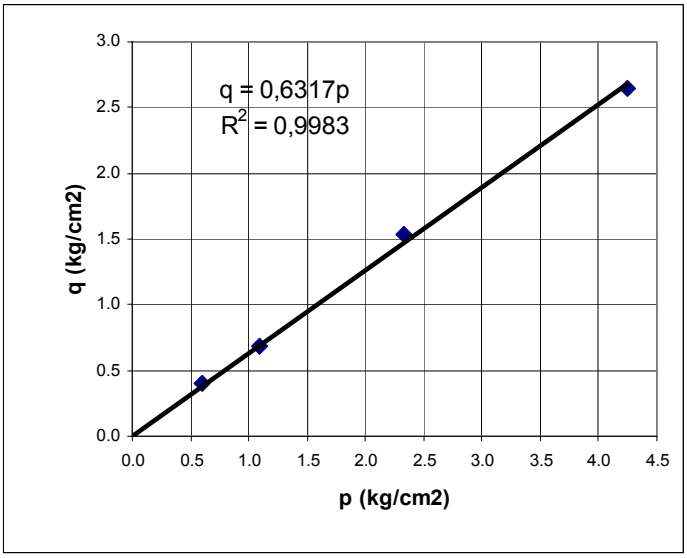

Figure 3.20: p-q diagram. DR = 35%.

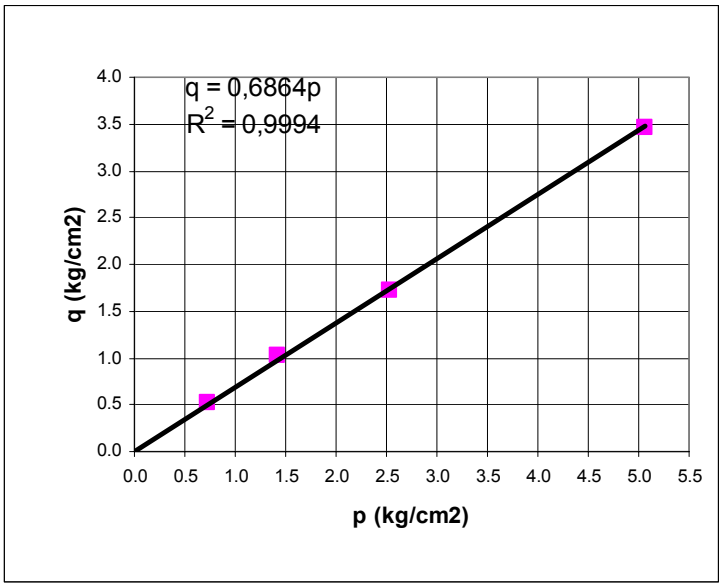

Figure 3.21: p-q diagram. DR = 55%.

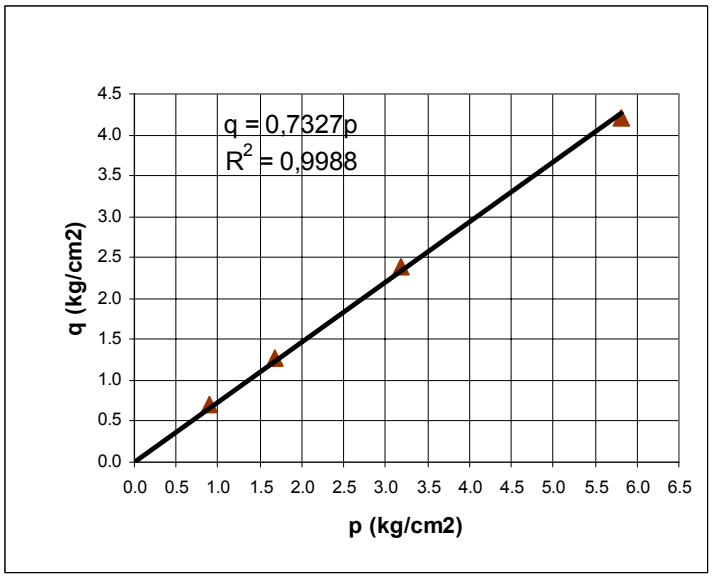

Figure 3.22: p-q diagram. DR = 75%.

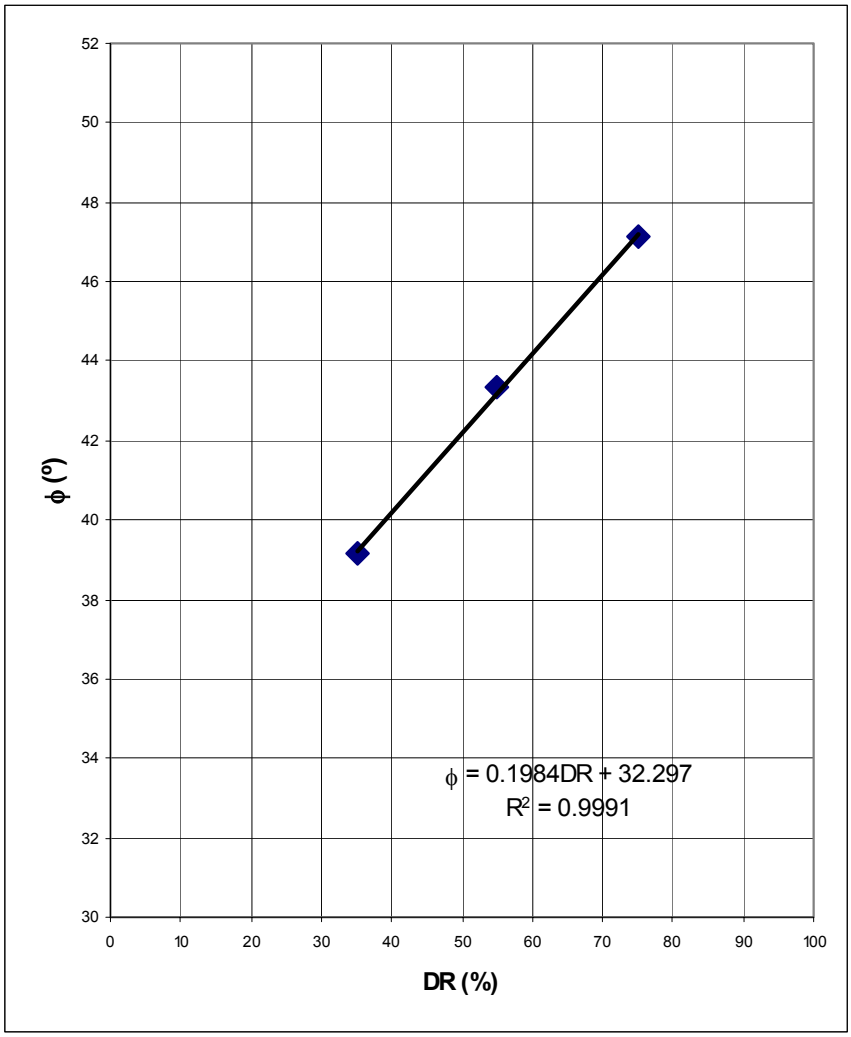

Figure 3.23: ϕ – DR .

IV. EXPERIMENTAL RESULTS.

4.1 Introduction.

The testing program included a series of circular and rectangular, smooth and rough bearing plates, with nil depth of footing measured from the sand surface, D_f.

The "smooth base" was assimilated to the condition existing in a polished machined steel to the bottom face of the bearing plate used. "Rough footings" were simulated by gluing sandpaper to the bottom with AGOREX 60. The sandpaper was an aluminium oxide cloth having a roughness grade of 40. The above procedure is similar to that used by Ko and Davidson in 1973, for rectangular plates tests.

50 test series were carried out (33 in smooth circular plate, 11 in rough circular plate, 4 in smooth rectangular plate and 2 in rough rectangular plate). 39 tests corresponding to values of relative densities of the sand tested over 53% are reported here.

In general, the results obtained are more consistent with some existing bearing capacity theories due to the markedly discrepancy that they present between them, in particular the evaluation of the parameter N_γ. In the following analysis the values of the angles of internal friction obtained from the triaxial tests have been applied in the different bearing capacity theories.

4.2 Analysis of the results obtained with circular footings.

4.2.1 Settlements analysis.

To have reliable results is necessary to meet two conditions: a) careful filling of the chamber (keeping the right control over the constant drop height), and b) precise installation of the bearing plate. Figure 4.1 shows the moment when the rectangular bearing plate is beinginstalled by hand over the sand. The rectangular plate was designed with two small handles to adequately move.

The circular plates used for testing are rigid steel plates 5, 7.5 and 10cm diameter (all of them 1.5cm thick) and 0.227, 0.552 and 0.949kg weight. The results obtained are summarized in the tables 4.1 and 4.2. The load-settlement curves are shown in the figures 4.2, 4.3 and 4.4, it can be noticed a peak strength value and then a decrease up to reach a residual strength value.

The start of the residual strength was reached with settlements values in the order of 1cm for the 5cm diameter smooth plate, 1.2cm for the 7.5cm diameter smooth plate and 1.5cm for the 10cm diameter smooth plate (see figures 4.2 and 4.3). The settlement in ultimate load (see table 4.1) increases when the plate's diameter increase. The settlement for the 5cm diameter smooth plate is ranging 0.35 to 0.45cm, for the 7.5cm diameter smooth plate is ranging 0.53 to 0.67cm, and for the 10cm diameter smooth plate is ranging 0.7 to 0.9cm. The small differences observed for the settlement values under ultimate load for each diameter plate are due to the variations in relative densities of the sand.

The start of the residual strength for the rough circular plates of 7.5cm diameter was reached in the range of settlement of 1.2 to 1.4cm (see figure 4.4), on the other hand the settlement corresponding to ultimate load was between 0.45 to 0.69cm (see table 4.2). For all the tests carried out with circular rough plate of 10cm diameter, the settlements were the 1.6cm at the begining of the residual strength and the settlements in ultimate load were 0.8 and 0.9cm.

4.2.2 Ultimate load analysis.

The stability of footings on sand is usually assessed applying limit equilibrium methods what consider independently the effect of self-weight in the failure zone and surcharge on the free surface.

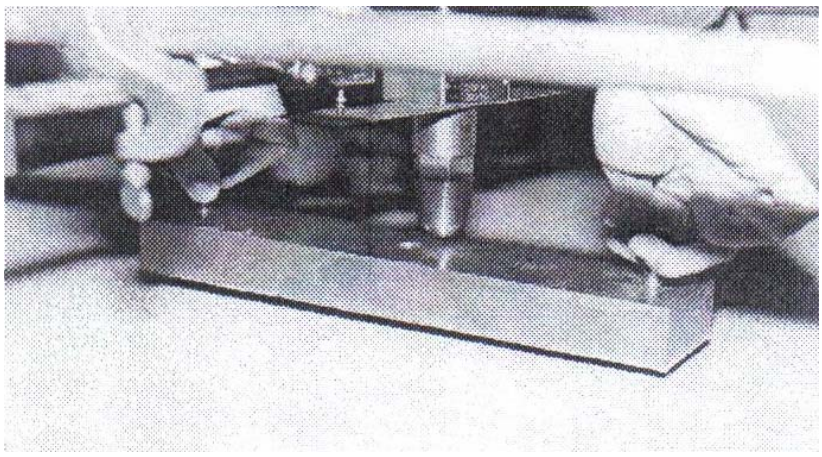

Figure 4.1: Installation of the rectangular plate in place for test. Note the small handles in the ends for a careful installation on the sand surface.

Table 4.1: Settlement in ultimate load for smooth circular plates.

TEST Nº	DATE	Diameter (cm)	area (cm2)	Q_u (Kg)	q_u (Kg/cm2)	q_u/pa	Settlement (cm)	γd average (T/m3)	γd (T/m3)	DR (%)	H (cm)
									1		
4	7/14/00	7.5	44.179	51.875	1.174	1.137	0.657	1.487	1.487	59	100
11	7/31/00	10.0	78.540	91.875	1.170	1.132	1.025	1.465	1.465	53	50
14	8/8/00	7.5	44.179	53.750	1.217	1.178	0.601	1.489	1.489	60	60
15	8/9/00	7.5	44.179	43.125	0.976	0.945	0.664	1.492	1.492	61	60
16	8/10/00	10	78.540	88.75	1.130	1.094	0.667	1.471	1.471	55	60
17	8/11/00	7.5	44.179	36.25	0.821	0.794	0.405	1.462	1.462	53	50
18	8/11/00	7.5	44.179	38.75	0.877	0.849	0.420	1.474	1.474	56	60
19	8/14/00	7.5	44.179	40.00	0.905	0.876	0.526	1.462	1.462	53	60
20	8/16/00	10	78.540	70.00	0.891	0.863	0.768	1.471	1.471	55	60
21	8/16/00	10	78.540	75.00	0.955	0.924	0.394	1.472	1.472	55	60
22	8/17/00	10	78.540	88.13	1.122	1.086	0.896	1.490	1.490	60	60
23	8/17/00	10	78.540	102.50	1.305	1.263	0.754	1.498	1.498	62	60
24	8/21/00	5	19.635	12.13	0.618	0.598	0.351	1.485	1.485	59	60
25	8/21/00	5	19.635	16.50	0.840	0.813	0.418	1.502	1.502	63	60
26(*)	8/22/00	10	78.540	82.50	1.050	1.017	0.571	1.476	1.476	56	60
27(*)	8/23/00	10	78.540	79.38	1.011	0.978	0.703	1.468	1.468	54	60
28	8/23/00	5	19.635	12.50	0.637	0.616	0.484	1.469	1.469	55	60
29(*)	8/24/00	10	78.540	73.75	0.939	0.909	0.684	1.485	1.485	59	60
30(**)	8/28/00	10	78.540	70.00	0.891	0.863	0.461	1.476	1.476	56	60
31	8/28/00	5	19.635	12.00	0.611	0.592	0.475	1.473	1.473	56	60
47	10/13/00	10	78.540	137.50	1.751	1.695	0.790	1.529	1.529	70	65
48	10/17/00	10	78.540	130.63	1.663	1.610	0.831	1.517	1.517	67	65

H: drop height of the sand

p_a = 1.033kg/cm^2: atmospheric pressure

(*): tests including one load-reload cycle

(**): tests including two load-reload cycle.

Table 4.2: Settlement in ultimate load for rough circular plates.

TEST	DATE	Diameter (cm)	area (cm2)	Q_u (Kg)	q_u (Kg/cm2)	q_u/pa	Settlement (cm)	γd average (T/m3)	γd (T/m3)	DR (%)	H (cm)
									1		
32	9/1/00	7.5	44.179	63.750	1.443	1.397	0.598	1.502	1.502	63	80
33	9/1/00	7.5	44.179	45.000	1.019	0.986	0.595	1.480	1.480	57	60
34	9/5/00	7.5	44.179	58.125	1.316	1.274	0.486	1.495	1.495	61	80
35	9/5/00	7.5	44.179	66.875	1.514	1.465	0.45	1.505	1.505	64	80
36	9/7/00	7.5	44.179	50.625	1.146	1.109	0.566	1.489	1.489	60	60
37	9/7/00	7.5	44.179	65.625	1.485	1.438	0.587	1.508	1.508	65	60
38	9/8/00	7.5	44.179	60.000	1.358	1.315	0.628	1.511	1.511	65	60
39	9/8/00	7.5	44.179	56.500	1.279	1.238	0.69	1.514	1.514	66	60
40	9/11/00	7.5	44.179	66.250	1.500	1.452	0.622	1.505	1.505	64	60
49	10/18/00	10	78.540	140.00	1.783	1.726	0.795	1.514	1.514	66	65
50	10/19/00	10	78.540	145.00	1.846	1.787	0.884	1.517	1.517	67	65

H: drop height of the sand

p_a = 1.033kg/cm^2: atmospheric pressure

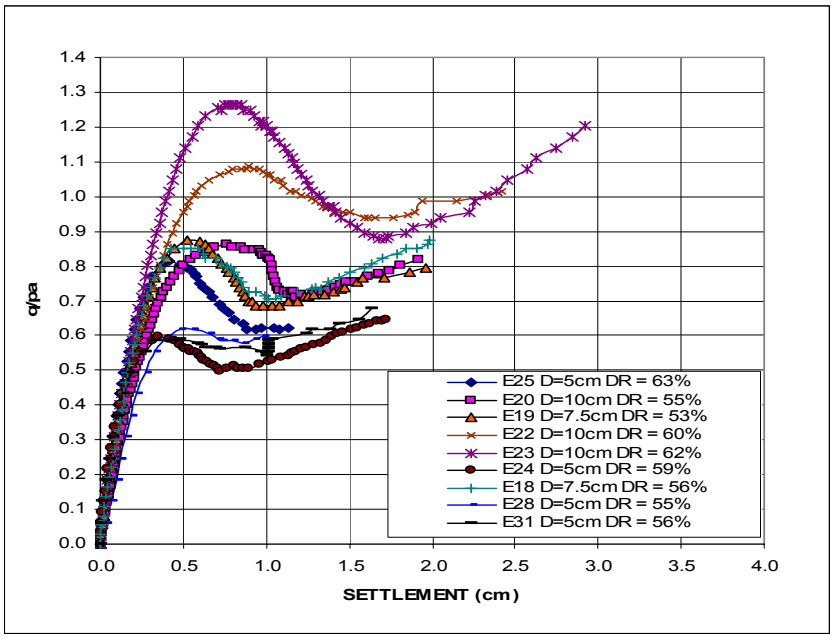

Figure 4.2: Load-settlement curves for smooth circular footings (I part).

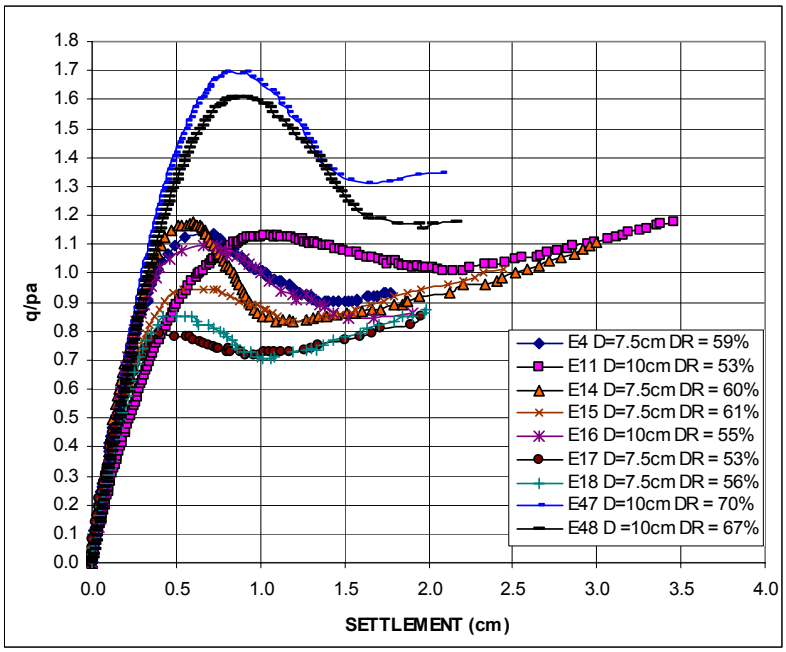

Figure 4.3: Load-settlement curves for smooth circular footings (II part).

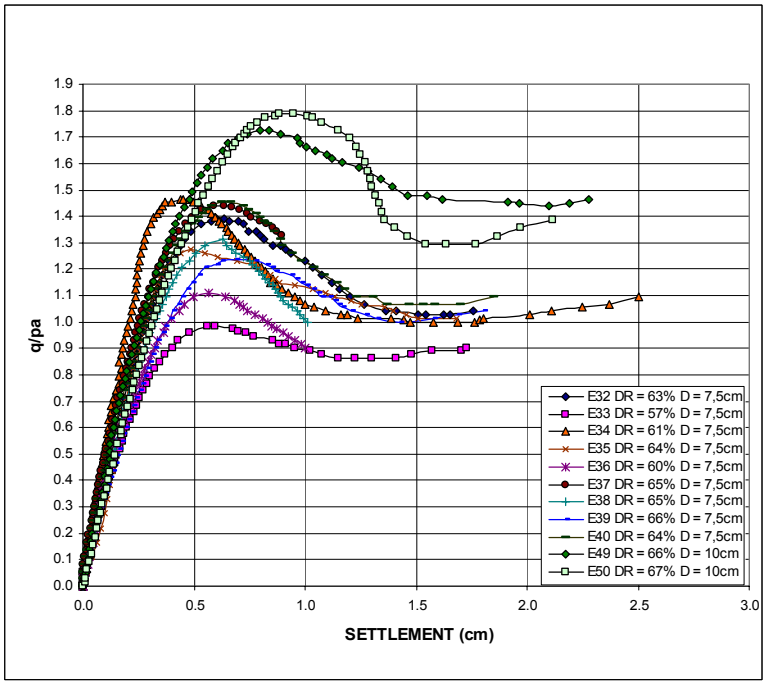

Figure 4.4: Load-settlement curves for rough circular footings.

Now, bearing in mind that there are two possibilities in the case of the ultimate bearing capacity determination through the experimental results: initial depth of footing $D_f = 0$ or the depth of footing in the ultimate bearing load trigger $D_f \neq 0$. There are usually no differences for this situation in the foundation engineering practice, however, the difference obtained in the tests was important. In consequence, the results obtained for the bearing capacity coefficient N_γ in both considerations above mentioned with relation to the value adopted by D_f are presented here. Thus, the following equations, in which the nomenclature used by N_γ in the (4.1b) equation was $N_{q\text{-}\gamma}$ with the purpose to avoid confusions in this respect were deducted.

$$N_\gamma = \frac{1}{0.5 s_\gamma d_\gamma \gamma B}\left(q_u - s_q d_q \gamma D_f N_q\right) \qquad (4.1a)$$

$$N_{q-\gamma} = \frac{q_u}{0.5 s_\gamma d_\gamma \gamma B} \qquad (4.1b)$$

The depth factor "d_γ" of the equation (4.1b) was adopted equal to 1 due to obviously the depth of footing is $D_f = 0$.

In the evaluation of the bearing capacity coefficient N_q, the equation (2.5) indicated in the second chapter was considered, using the angle of internal friction provided by the equation (3.3), in terms of the relative density of the sand.

Tables 4.3a and 4.3b show the results obtained considering the shape and depth factors proposed by Terzaghi (1943) in the equations (4.1a and 4.1b) for the cases of circular smooth and rough plates respectively. Indeed, it was observed that the factor $N_{q\text{-}\gamma}$ overestimates significantly the parameter N_γ. Therefore, it definitively was adopted the equation 4.1a for the evaluation of the coefficient N_γ.

Table 4.3a: Smooth circular load plates. Comparison of measured bearing capacity factors N_γ and $N_{q\text{-}\gamma}$.

TEST Nº	ϕtx (º)	ϕpl (º)	Nq	Nq-γ	Nγ
4	44.1	44.1	116.41	350.96	316.96
11	42.9	42.9	97.51	266.16	232.85
14	44.2	44.2	118.30	363.15	331.55
15	44.3	44.3	121.20	290.78	255.01
16	43.2	43.2	102.33	256.06	233.31
17	42.7	42.7	95.18	249.44	232.31
18	43.4	43.4	104.83	264.47	244.90
19	42.7	42.7	95.18	275.24	252.99
20	43.2	43.2	102.33	201.96	175.77
21	43.3	43.3	103.16	216.24	202.70
22	44.2	44.2	119.26	251.02	215.40
23	44.6	44.6	127.21	290.40	258.43
24	44.0	44.0	114.54	277.23	250.42
25	44.8	44.8	131.39	372.99	336.37
28	43.1	43.1	100.70	288.91	256.42
31	43.3	43.3	103.99	276.60	243.67
47	46.2	46.2	163.53	381.67	338.60
48	45.6	45.6	148.35	365.45	324.36

Table 4.3b: Rough circular load plates. Comparison of measured bearing capacity factors N_γ and $N_{q\text{-}\gamma}$.

TEST Nº	ϕtx (º)	ϕpl (º)	Nq	Nq-γ	Nγ
32	44.8	44.8	131.39	426.99	392.07
33	43.7	43.7	110.02	305.88	276.79
34	44.5	44.5	124.17	391.14	364.31
35	45.0	45.0	134.62	447.03	420.10
36	44.2	44.2	118.30	342.04	312.28
37	45.1	45.1	137.93	437.80	401.81
38	45.3	45.3	141.32	399.48	360.03
39	45.4	45.4	144.79	375.43	331.03
40	45.0	45.0	134.62	442.85	405.63
49	45.4	45.4	144.79	392.46	354.08
50	45.6	45.6	148.35	405.67	361.95

Tables 4.4a and 4.4b show and allow to make a comparison the experimental values obtained by N_γ, according to equation 4.1a, defined for the shape and depth factors by the different authors considered with the values of N_γ gave for the equations (2.7), (2.8) and (2.9) belonging to second chapter. The theoretical N_γ proposed by Vesic (1973), Meyerhof (1963) and Hansen (1970), were calculated in terms of the angle ϕ_{tx}. With respect to the theoretical Terzaghi's N_γ, also included in such tables, they were calculated from the values tabulated by Kumbhojkar (1993) for intervals of ϕ equals to 0.5º.

As a way to analyse the whole results, the different testing curves for circular rough and smooth footings for all the diameters tested as well as for rectangular rough and smooth footings (analysed in the point 4.3) were summarized and plotted in a same graph.

Calculations of N_γ have been tabulated in tables 4.4a and 4.4b and then plotted against the angle of internal friction ϕ_{tx} in the figures 4.5 to 4.8 for the four authors above mentioned, with the purpose to contrast the experiments against the diverse existing theories for smooth and rough footings. From the graph inspection it can be noticed that the Terzaghi's theory gets the best fit to the experiments values among the others. In second place one can appreciate that Vesic's theory gets a good fit too. Specially, the Terzaghi's theory for the case of rough footing approximates very good to circular as well as strip footings. On the other hand, Vesic's theory fits better to the case of smooth footings. The astonishing case corresponds to the Terzaghi's theory, established from 1943. Figure 4.8 shows the unbelievable fit of the calculated experimental values corresponding to the Terzaghi's formula and parameters with the values predicted by the same Terzaghi's theory. The fact that could be explain this situation is maybe due to Terzaghi (1943) used only the shape factors, which have consistence with the shallow plates tested (without depth factors). Moreover, the Terzaghi's N_γ values were deduced for the case of rough footings, which in general adjust much better to the physical reality owing to the smooth case have only a theoretical worth.

Table 4.4a: Smooth circular load plates. Comparison of theoretical and measured bearing capacity factor N_γ.

	Terzaghi(1943)		Vesic(1973)		Meyerhof(1963)		B.Hansen(1970)	
TEST Nº	Nγ Theoretical	Nγ Testing	Nγ Theoretical	Nγ Testing	Nγ Theoretical	Nγ Testing	Nγ Theoretical	Nγ Testing
4	272	316.96	227.24	283.02	214.21	170.53	167.53	292.42
11	210	232.85	183.06	200.65	167.54	125.63	134.51	209.08
14	278	331.55	231.75	299.97	219.05	178.61	170.90	308.77
15	288	255.01	238.67	218.97	226.53	136.45	176.07	229.07
16	226	233.31	194.19	211.38	179.14	126.64	142.82	217.25
17	203	232.31	177.73	216.14	162.02	126.93	130.53	220.38
18	234	244.90	200.00	226.02	185.24	133.17	147.17	231.12
19	203	252.99	177.73	231.86	162.02	137.83	130.53	237.39
20	226	175.77	194.19	150.42	179.14	94.83	142.82	157.20
21	228	202.70	196.11	189.75	181.15	110.61	144.26	193.24
22	282	215.40	234.03	179.62	221.52	115.02	172.61	189.59
23	309	258.43	253.14	226.03	242.28	138.41	186.90	235.25
24	266	250.42	222.83	223.91	209.47	135.08	164.23	231.24
25	323	336.37	263.27	298.91	253.38	180.01	194.47	309.65
28	220	256.42	190.41	224.86	175.19	138.45	140.00	233.22
31	231	243.67	198.05	211.48	183.19	131.29	145.71	220.10
47	437	338.60	343.01	292.59	343.30	179.03	254.13	306.58
48	383	324.36	304.97	281.25	299.88	172.25	225.66	294.02

Table 4.4b: Rough circular load plates. Comparison of theoretical and measured bearing capacity factor N_γ.

	Terzaghi(1943)		Vesic(1973)		Meyerhof(1963)		B.Hansen(1970)	
TEST Nº	Nγ Theoretical	Nγ Testing	Nγ Theoretical	Nγ Testing	Nγ Theoretical	Nγ Testing	Nγ Theoretical	Nγ Testing
32	392.07	323	263.27	356.38	253.38	210.36	194.47	366.62
33	276.79	251	212.15	248.17	198.09	149.46	156.25	255.98
34	364.31	298	245.80	337.37	234.27	196.60	181.41	345.00
35	420.10	334	271.13	392.63	262.06	226.24	200.35	400.59
36	312.28	278	231.75	282.58	219.05	168.31	170.90	290.86
37	401.81	346	279.22	364.69	271.03	215.13	206.40	375.49
38	360.03	358	287.55	319.06	280.32	192.00	212.63	331.05
39	331.03	370	296.13	284.55	289.93	175.66	219.05	298.21
40	405.63	334	271.13	367.37	262.06	217.26	200.35	378.42
49	354.08	370	296.13	314.08	289.93	188.72	219.05	325.86
50	361.95	383	304.97	316.02	299.88	192.22	225.66	329.62

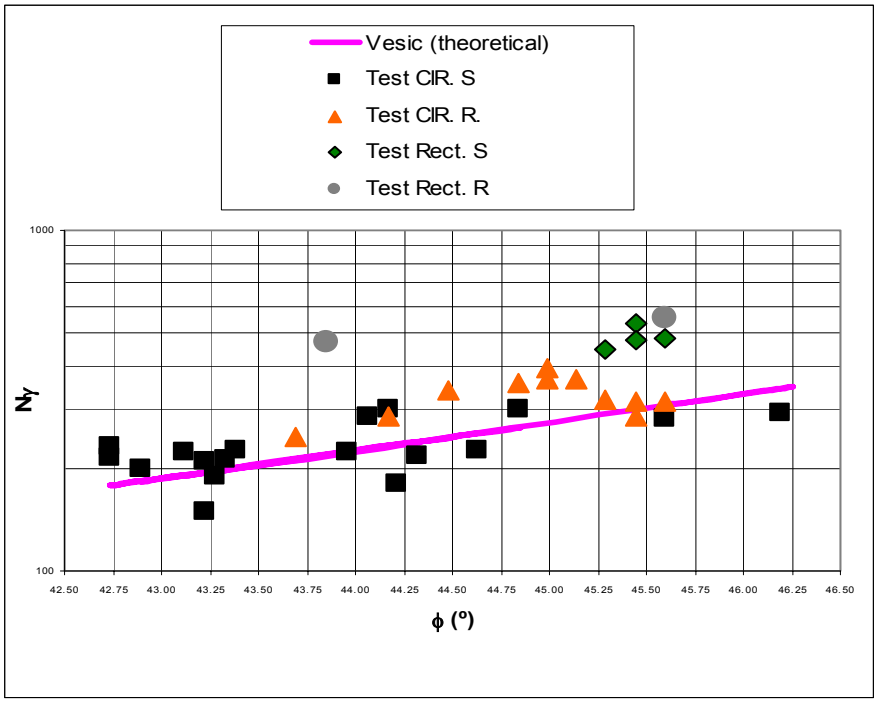

Figure 4.5: Factor N_γ after Vesic (1973) versus ϕ.

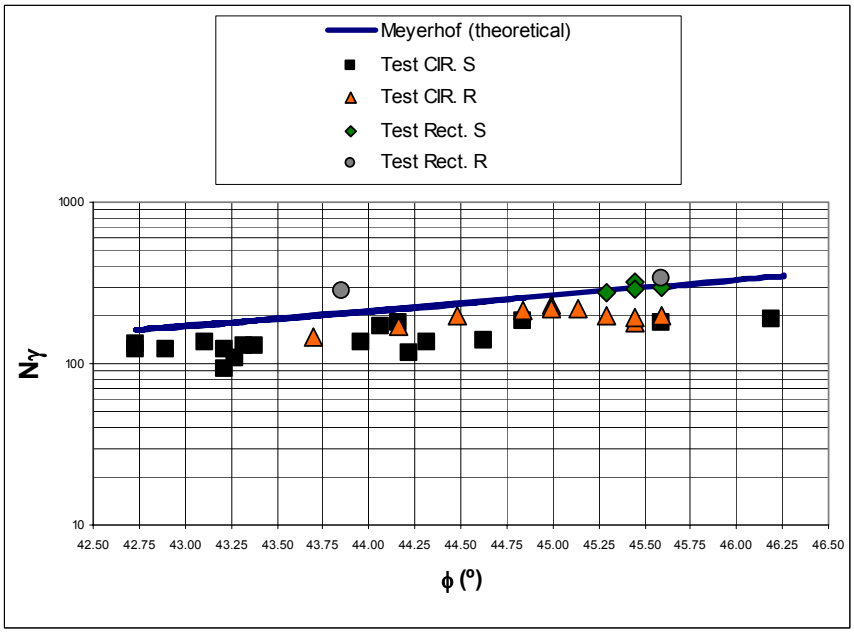

Figure 4.6: Factor N_γ after Meyerhof (1963) versus ϕ.

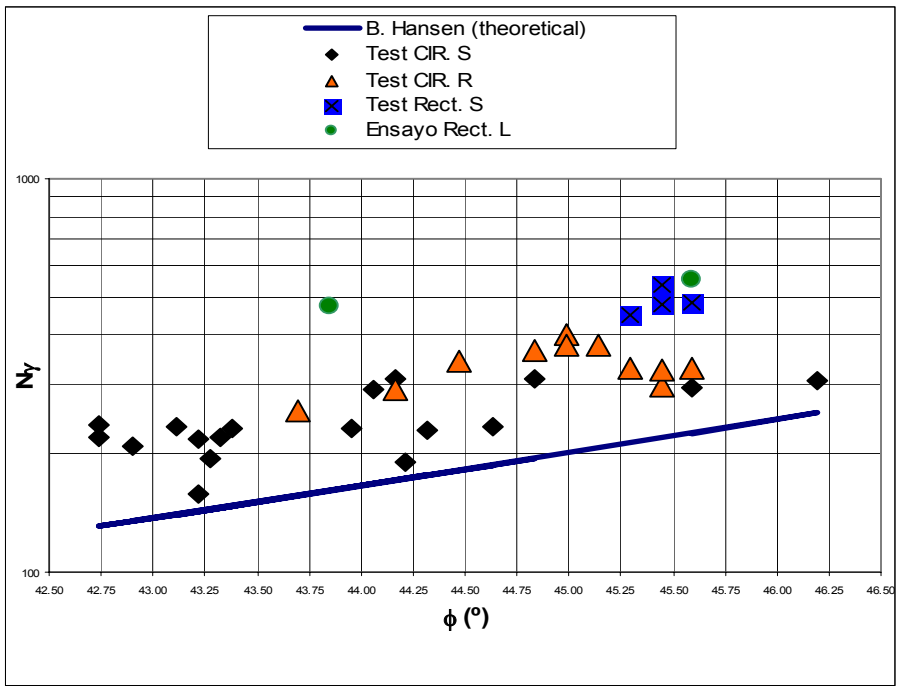

Figure 4.7: Factor N_γ after Brich Hansen (1970) versus ϕ.

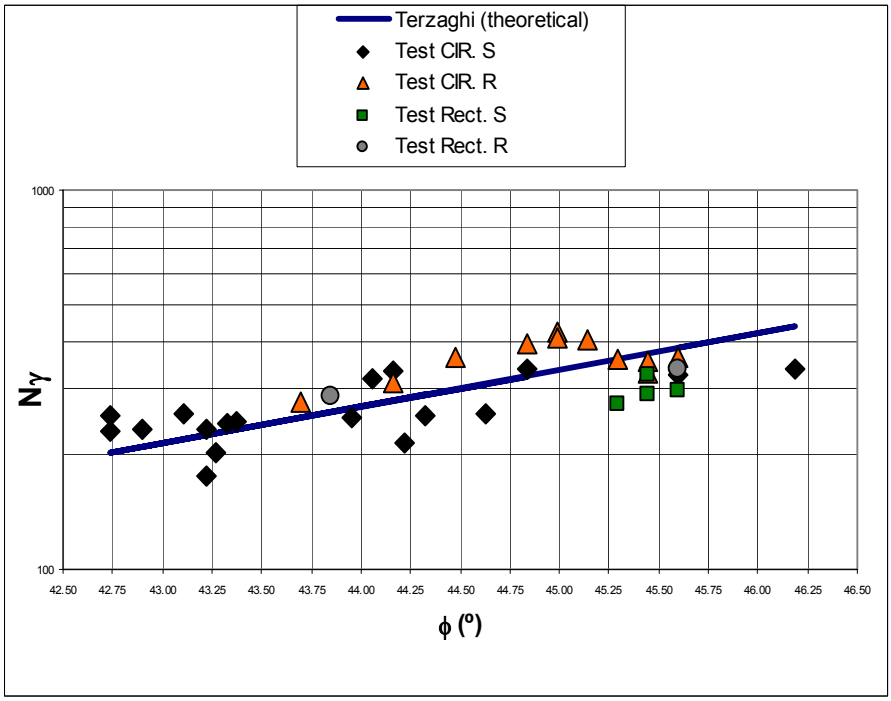

Figure 4.8: Factor N_γ after Terzaghi (1943) versus ϕ.

The fit shown in the figure 4.6 for the Meyerhof's N_γ formula with their respective shape and depth factors is slight over the values obtained from the tests. It's notable (*i*) the relatively low scattering of the experimental values and (*ii*) the similarity of the Meyerhof's formula and the experimental points. It is possible to note the low increase of N_γ by the rough bottom footing effect in the testing values, being not understandable the recommendation proposed by Meyerhof in order to reduce in a half the failure load for smooth footings.

The application of the Brinch Hansen's theory gives bearing capacities (N_γ) smaller than those observed in the laboratory, indicating this theory would be very conservative for the Brinch Hansen's parameter N_γ. Another reason for the N_γ values could be the shape and depth factors, making necessary some adjustment to these factors for small values of D_f.

Based on data from table 4.5 and 4.6, figures 4.9 and 4.10 were prepared. Both the average and experimental values are shown for each author and for each kind of footing (circular smooth and rough). A comparison with predictive ultimate bearing capacity equations by the four authors can be made for the footings tested using these figures. In both figures, a linear variation plotted through the experimental points looks reasonable, thus confirming the good similarity between the experimental evidence with the Terzaghi's theory. It's interesting to compare the predictions in base of the N_γ values analysis for the four authors. Vesic and Terzaghi are who have theories closer to the experimental results for the circular smooth and rough footings.

In spite of the great scattering of the results, these show a clear trend within the graph for each author in figure 4.9 and 4.10.

Although N_γ is a dimensionless value, N_γ calculated from the loadings tests of footings on sand decreases as increasing footing size (De Beer, 1970; Kimura *et al*., 1985; Ueno *et al*., 1998). This phenomenon is referred to as the size effects of footing width on the bearing capacity factors. One of the reasons is that for wider footings the stress level are

greater too in their failure zones, mobilized ϕ values are smaller in failure zones and consequently N_γ values are lower. While N_γ is expected to be constant independent of the variation of B from the original meaning of the Terzaghi's bearing capacity formula (equation 2.10). The above qualitative discussion suggests that N_γ decreases as B increases. The scattering of the ultimate bearing capacity ratio above mentioned (figures 4.9 and 4.10) could be explained in part due to the fact that N_γ depends not only of the angle ϕ, but also is proportional to the width of footing B.

Table 4.5: Ultimate load in tests of smooth circular plates. (q_u in kg/cm^2).

		Vesic (1973)				Meyerhof (1963)				B.Hansen (1970) (**)			Terzaghi (1943)	
TEST	qu	sγ = 0.6		dγ = 1						sγ = 0.6		dγ = 1	sγ = 0.6	
Nº	TEST	sq	dq	qu	(*)	sq=sγ	dq=dg	qu	(*)	sq	qu	(*)	qu	(*)
4	1.17	1.97	1.02	0.99	**0.84**	1.09	1.01	1.44	**1.23**	1.70	0.76	**0.64**	1.02	**0.87**
11	1.17	1.93	1.02	1.09	**0.93**	1.09	1.01	1.51	**1.29**	1.68	0.84	**0.72**	1.07	**0.91**
14	1.22	1.97	1.01	0.99	**0.81**	1.09	1.01	1.47	**1.20**	1.70	0.75	**0.62**	1.04	**0.85**
15	0.98	1.98	1.02	1.04	**1.07**	1.10	1.01	1.53	**1.57**	1.70	0.80	**0.82**	1.09	**1.11**
16	1.13	1.94	1.01	1.05	**0.93**	1.09	1.01	1.55	**1.37**	1.68	0.80	**0.71**	1.10	**0.97**
17	0.82	1.92	1.01	0.69	**0.85**	1.09	1.00	1.03	**1.26**	1.68	0.52	**0.64**	0.72	**0.88**
18	0.88	1.94	1.01	0.79	**0.90**	1.09	1.01	1.19	**1.36**	1.69	0.60	**0.68**	0.84	**0.96**
19	0.91	1.92	1.01	0.73	**0.80**	1.09	1.01	1.05	**1.16**	1.68	0.55	**0.61**	0.74	**0.82**
20	0.89	1.94	1.01	1.08	**1.22**	1.09	1.01	1.57	**1.76**	1.68	0.83	**0.93**	1.11	**1.25**
21	0.95	1.94	1.01	0.98	**1.03**	1.09	1.00	1.52	**1.59**	1.69	0.74	**0.77**	1.07	**1.12**
22	1.12	1.97	1.02	1.37	**1.22**	1.09	1.01	2.00	**1.78**	1.70	1.05	**0.93**	1.42	**1.26**
23	1.31	1.99	1.01	1.43	**1.09**	1.10	1.01	2.17	**1.66**	1.70	1.09	**0.83**	1.53	**1.17**
24	0.62	1.96	1.01	0.62	**1.00**	1.09	1.01	0.92	**1.49**	1.69	0.47	**0.76**	0.65	**1.06**
25	0.84	1.99	1.01	0.76	**0.90**	1.10	1.01	1.15	**1.36**	1.71	0.58	**0.69**	0.81	**0.96**
28	0.64	1.94	1.02	0.56	**0.88**	1.09	1.01	0.78	**1.23**	1.68	0.43	**0.68**	0.56	**0.87**
31	0.61	1.94	1.02	0.58	**0.95**	1.09	1.01	0.82	**1.34**	1.69	0.45	**0.73**	0.58	**0.95**
47	1.75	2.04	1.01	1.98	**1.13**	1.11	1.01	3.15	**1.80**	1.72	1.51	**0.86**	2.20	**1.26**
48	1.66	2.02	1.01	1.77	**1.06**	1.10	1.01	2.74	**1.65**	1.71	1.35	**0.81**	1.93	**1.16**

(*): q_u theory/ q_u experimental

(**): d_q (Hansen) = d_q (Vesic)

Table 4.6: Ultimate load in tests of rough circular plates. (q_u in kg/cm^2).

Test Nº	qu Test	Vesic (1973) sγ = 0.6 dγ = 1 sq	dq	qu	(*)	Meyerhof (1963) sq=sγ	dq=dγ	qu	(*)	B. Hansen (1970) (**) sγ = 0.6 dγ = 1 sq	qu	(*)	Terzaghi (1943) sγ = 0.6 qu	(*)
32	1.443	1.994	1.01	1.128	**0.78**	1.10	1.01	1.711	**1.19**	1.705	0.861	**0.60**	1.21	**0.84**
33	1.019	1.955	1.01	0.899	**0.88**	1.09	1.01	1.315	**1.29**	1.691	0.686	**0.67**	0.93	**0.92**
34	1.316	1.982	1.01	1.008	**0.77**	1.10	1.01	1.549	**1.18**	1.701	0.765	**0.58**	1.09	**0.83**
35	1.514	2.000	1.01	1.102	**0.73**	1.10	1.01	1.737	**1.15**	1.707	0.836	**0.55**	1.22	**0.81**
36	1.146	1.971	1.01	0.976	**0.85**	1.09	1.01	1.458	**1.27**	1.697	0.744	**0.65**	1.03	**0.90**
37	1.485	2.005	1.01	1.195	**0.80**	1.10	1.01	1.836	**1.24**	1.709	0.912	**0.61**	1.30	**0.87**
38	1.358	2.010	1.01	1.251	**0.92**	1.10	1.01	1.914	**1.41**	1.711	0.956	**0.70**	1.35	**0.99**
39	1.279	2.016	1.02	1.318	**1.03**	1.10	1.01	2.001	**1.56**	1.713	1.009	**0.79**	1.41	**1.10**
40	1.500	2.000	1.01	1.174	**0.78**	1.10	1.01	1.780	**1.19**	1.707	0.897	**0.60**	1.26	**0.84**
49	1.783	2.016	1.01	1.701	**0.95**	1.10	1.01	2.635	**1.48**	1.713	1.297	**0.73**	1.85	**1.04**
50	1.846	2.021	1.01	1.796	**0.97**	1.10	1.01	2.756	**1.49**	1.714	1.373	**0.74**	1.94	**1.05**

(*): q_u theory/ q_u experimental

(**): d_q (Hansen) = d_q (Vesic)

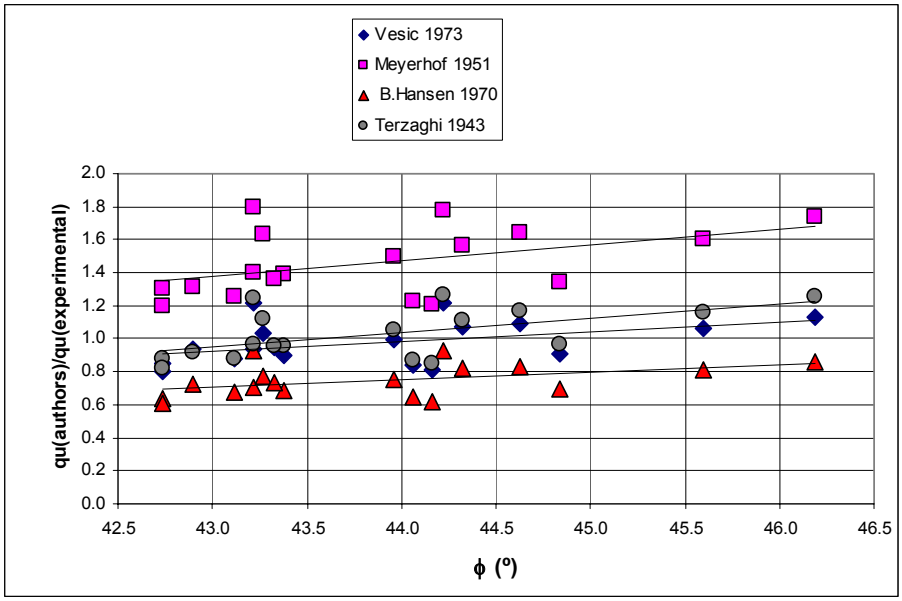

Figure 4.9: q_u(authors)/ q_u(experimental) ratio. Smooth circular footings.

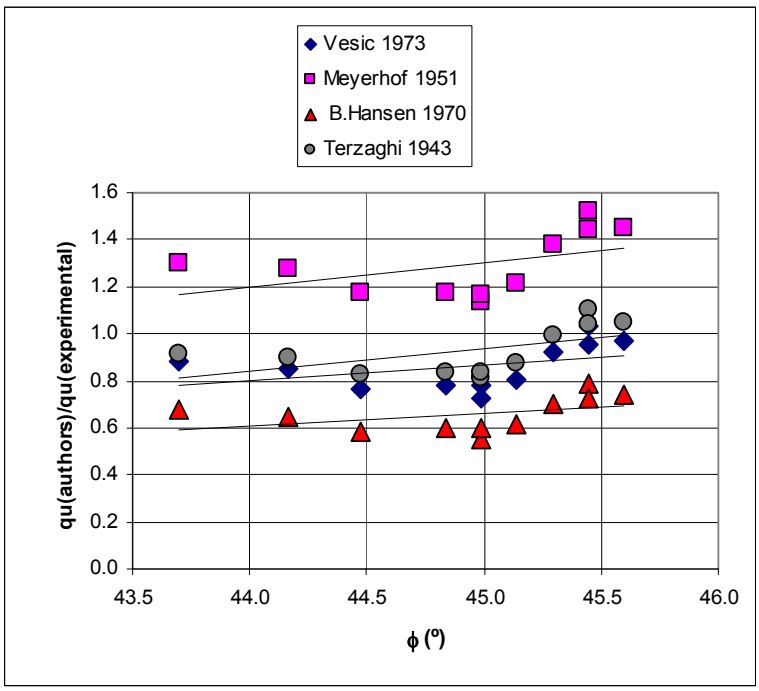

Figure 4.10: q_u(authors)/ q_u(experimental) ratio. Rough circular footings.

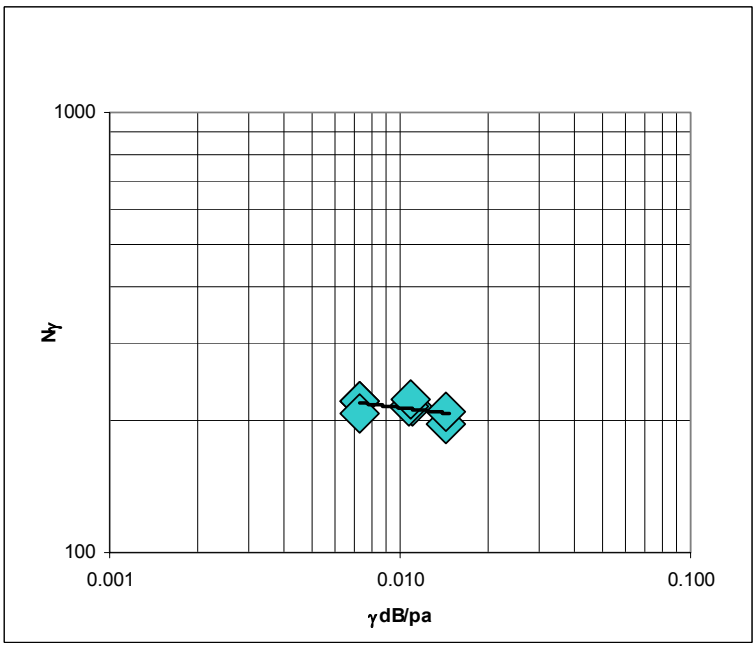

Figure 4.11: N_γ versus $\gamma_d B/p_a$. Smooth circular footings.

Figure 4.11 shows the logarithmic relationships between N_γ and normalized footing width $\gamma_d B/p_a$ obtained from some test series in the present research. The normalization for the width of footing $\gamma_d B/p_a$ allows to demonstrate the size effect on bearing capacity, based on the results from the model tests. The plots of $\log N_\gamma$ against $\log \gamma_d B/p_a$ with negative correlation indicate, for circular smooth footings, a reduction in N_γ with increasing B, with N_γ determination in base to the equation 4.1a using the Terzaghi's shape factors and the plate diameter. Many prediction methods (Numerical analysis methods-finite element method, for example) have been proposed with regard to the size effects, however, the applicability of these proposed methods needs procedures that should be easy to use in foundation engineering. The size effects are caused by confining stress level effects on shear strength, progressive failure of foundation grounds and the scale effects of footing width with respect to the particle size of ground materials. Ovesen (1979) commented that the scale effect is emphasized only in small scaled footings whose footing width B is less than 30 times the grain size of foundation ground material (d_{50}).

4.2.3 Load-settlement curves with unloading-reloading cycles.

In the cyclic tests the same velocity of loading applied before was used, i.e., 1mm/min. The filling of the chamber was done applying the sand pluviation method. The only difference was the application of an unloading and then a reloading over the sand tested before to reach the ultimate load.

Figures 4.12, 4.13, 4.14 and 4.15 shown the load-settlement curves with one unloading-reloading cycle for the three first figures and two unloading-reloading cycles for the last figure. It can be noted the effect of unloading-reloading cycle in the ultimate bearing capacity results, where in general, there is a diminution if it compares with a test without unloading-reloading cycle. In fact, for equal relative density, for example the figures 4.12 and 4.15 correspond respectively to 56% and 57% relative density, it can be noted the reduction of the ultimate load in the test with two cycles respecting to the tests with only one cycle. Alternatively, it can be noted the notorious elastic-lineal behaviour during the unloading-loading processes with slopes approximately parallels and steeper than the initial slopes of the

load-settlement curves. Nevertheless, it not possible quantified this results due to the few number of unloading-loading tests made. The analysis of this aspect had a secondary interest respecting to the objective of the present research and therefore it is beyond the scope of this thesis.

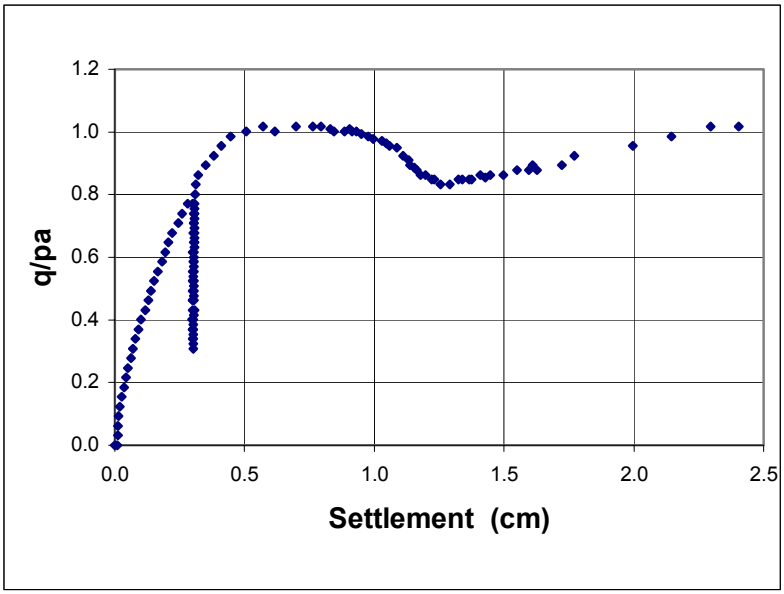

Figure 4.12: Test 26: Circular load plate diameter 10cm (smooth)

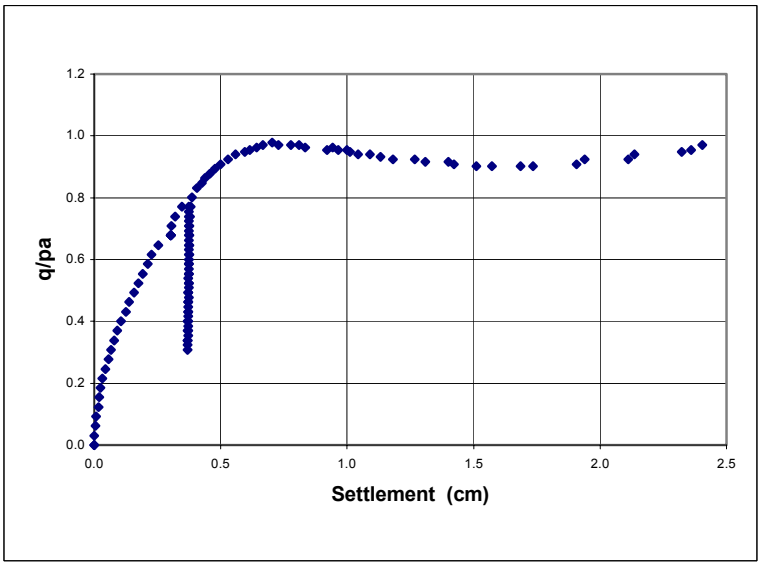

Figure 4.13: Test 27: Circular load plate diameter 10cm (smooth)

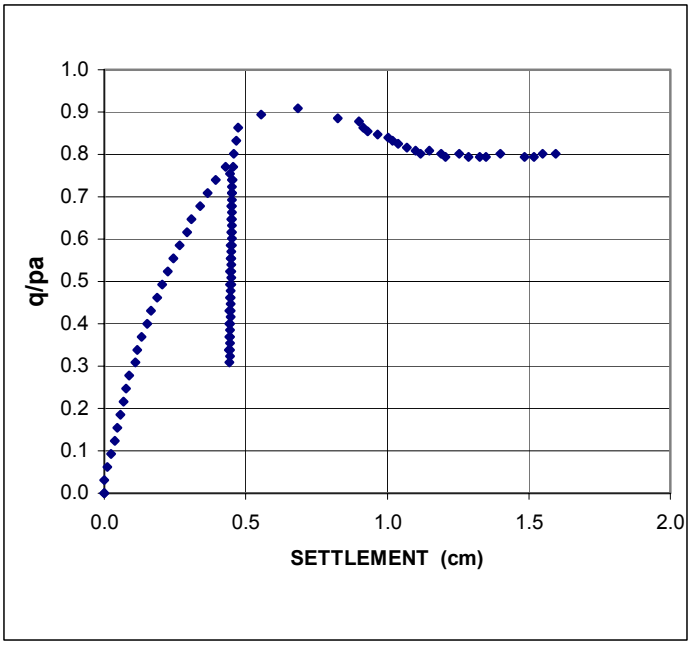

Figure 4.14: Test 29: Circular load plate diameter 10cm (smooth)

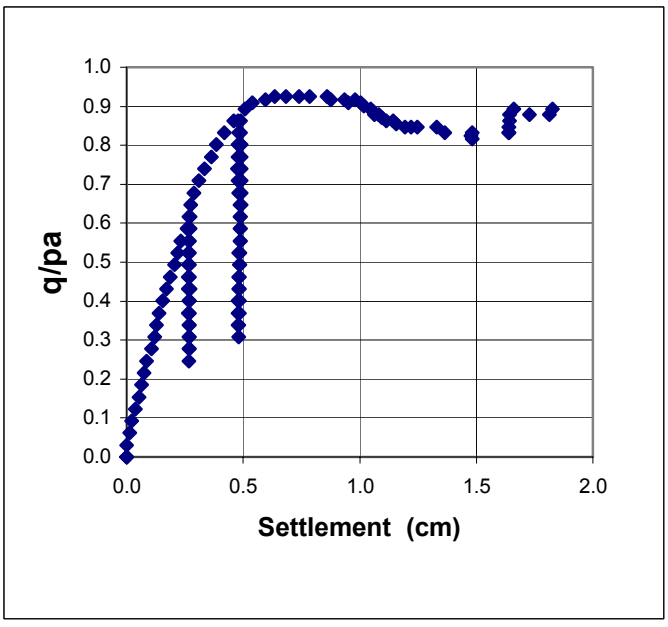

Figure 4.15: Test 30: Circular load plate diameter 10cm (smooth)

4.3 Results analysis obtained with rectangular footings.

4.3.1 General aspects.

The purpose of this part of the investigation is to compare the ultimate bearing capacity as predicted by the theory's solution with the results obtained from plane strain ultimate bearing capacity tests on smooth footings and, besides, to examine the effect of footing roughness on ultimate bearing capacity. The size of the steel strip footing used was 30cm long and 6cm wide, i.e., a ratio L/B = 5. Such ratio is usually assumed as approximately representative for a strip foundation. The thickness of the footing used was 3.5cm.

The surface the presence of failure patterns in all these tests was observed on the surface. In general, the intersections of the failure planes with the surface of the sand were clearly visible. The significant difference between the patterns for the circular and strip footing shapes is – superficially noticed - the mobilization of the failure pattern around the strip footing which does not occur around the circular one. In the strip footings tests one- sided failure patterns were produced. Such pattern was hardly seen at the end of the test when the settlements were associated with the residual strength. At the moment when the residual strength of the footings were reached, differential settlements of the sand surface began to indicate the failure zone. With increased settlements of the footing beyond this point it was evident from the surface settlements that, in general, the location of the failure surface did not change. The failure pattern had length of 6 to 7 times the width of the footing measured from the edge of the footing.

4.3.2 Settlements analysis.

The values of the settlements and other data of the static experiments are summarized in tables 4.7a and 4.7b. For the smooth plate the settlement ranged from 0.57 to 0.66cm for an average relative density of 66% and for the rough plate the settlement was 0.55 for a relative density of 58% and 0.67cm for 67%. Figure 4.16 shows essentially the same load-settlement curves shape, that is, an initial peak followed by a valley. The general

behaviour of strip footings differs from the circular footings in that when one wishes to consider the peak of failure, the fact was that in the first case the peak have a sharp shape and in the second the peak have a smoother shape, like a gaussian curve (see figures 4.2 to 4.4).

The settlements corresponding to the initial residual strength are in the range of 1.0 to 1.5cm for the six tests carried out. In this investigation attention will deal primarily with the maximum bearing capacities because they are of more general interest.

Table 4.7a: Settlement in ultimate load for smooth strip plates.

TEST	DATE	B (cm)	Area (cm2)	Qu (Kg)	qu (Kg/cm2)	qu/pa	Settlement (cm)	γd average (T/m3)	γd (T/m3)	DR (%)	H (cm)
41	9/21/00	6	180	290.0	1.611	1.560	0.568	1.514	1.514	66	60
42	9/1/00	6	180	266.8	1.482	1.435	0.592	1.517	1.517	67	60
43	9/5/00	6	180	261.0	1.450	1.404	0.583	1.514	1.514	66	60
44	9/5/00	6	180	249.4	1.386	1.341	0.664	1.511	1.511	65	60

Table 4.7b: Settlement in ultimate load for rough strip plates.

TEST	DATE	B (cm)	Area (cm2)	Qu (Kg)	qu (Kg/cm2)	qu/pa	Settlement (cm)	γd average (T/m3)	γd (T/m3)	DR (%)	H (cm)
45	9/7/00	6	180	304.500	1.692	1.638	0.671	1.517	1.517	67	65
46	9/7/00	6	180	246.500	1.369	1.326	0.553	1.483	1.483	58	70

H: drop height of the sand

$p_a = 1.033 kg/cm^2$: atmospheric pressure

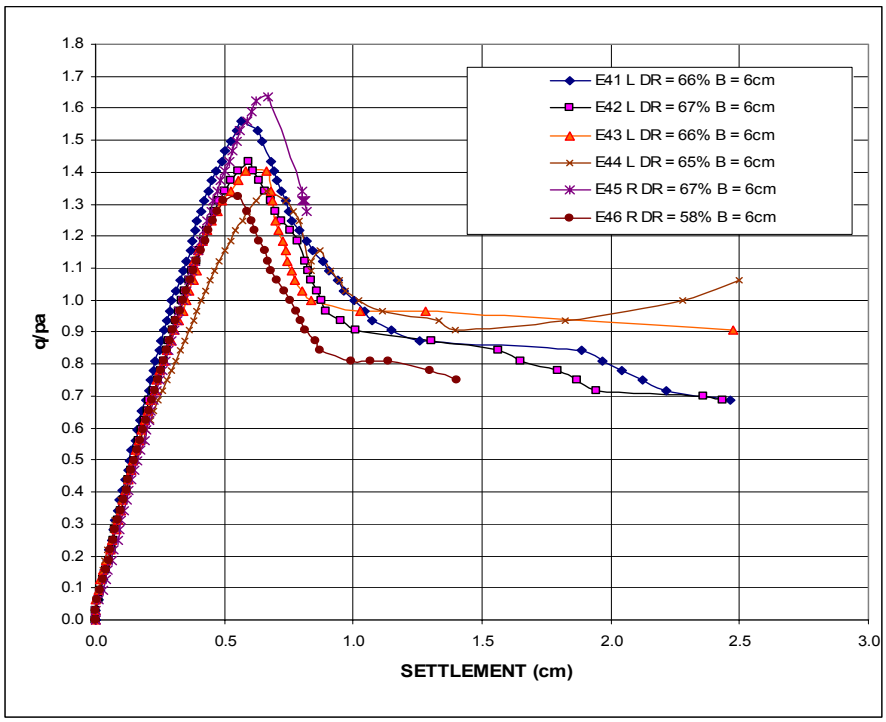

Figure 4.16: Load-settlement curves for smooth (L) and rough (R) strip footing.

4.3.3 Analysis of the bearing capacity.

The experimentally determined ultimate bearing capacities represent as the maximum pressure from the static load-settlement curves can be compared with the available theoretical formulas. In the same way, as before for circular plates, all comparisons will be made with the approximate theories by Terzaghi (1943), Vesic (1973), Meyerhof (1963) and Hansen (1970). These formulas are perhaps the best known, and have been most frequently used for comparison with other available data and theories. The calculation of the dimensionless bearing capacity factor N_γ was made using the equations 4.1a and 4.1b.

Tables 4.8a and 4.8b summarize the results for smooth and rough plates respectively. It was noted again that the factors $N_{q\text{-}\gamma}$ are significantly higher than the factors N_γ, and thus, the consideration of the depth D_f (settlement) of the footing in the instant of ultimate load is an important aspect in a rigorous analysis of the experimental results.

The resultant values of N_γ against ϕ, corresponding to the strip plates are included in tables 4.9a and 4.9b, and in figures 4.5 to 4.8. This confirms that the Terzaghi's theory (1943) is the best fit to the physical reality to rough footings. In the case of smooth footings, the Meyerhof's theory (1963) gives a better approximation. This conclusion can be verified in figures 4.17 and 4.18, in where the values of the measured bearing capacity and the values computed by the different theories against the angle of internal friction of the sand tested were plotted.

Table 4.8a: Smooth strip load plates. Comparison of measured bearing capacity factors N_γ and $N_{q\text{-}\gamma}$.

TEST	ϕ_{tx} (º)	ϕ_{pl} (º)	Nq	Nq-γ	Nγ
41	45.4	45.4	144.79	354.71	327.30
42	45.6	45.6	148.35	325.69	296.42
43	45.4	45.4	144.79	319.24	291.10
44	45.3	45.3	141.32	305.66	274.38

Table 4.8b: Rough strip load plates. Comparison of measured bearing capacity factors N_γ and $N_{q\text{-}\gamma}$.

TEST	ϕ_{tx} (º)	ϕ_{pl} (º)	Nq	Nq-γ	Nγ
45	45.6	45.6	148.35	371.71	338.53
46	43.9	43.9	112.71	307.81	287.03

Table 4.9a: Smooth strip load plates. Comparison of theoretical and measured bearing capacity factor N_γ.

	Terzaghi (1943)		Vesic (1973)		Meyerhof(1963)		B. Hansen(1970)	
TEST Nº	Nγ Theoretical	Nγ Testing	Nγ Theoretical	Nγ Testing	Nγ Theoretical	Nγ Testing	Nγ Theoretical	Nγ Testing
41	370	327.3	296.13	535.35	289.93	316.82	219.05	538.16
42	383	296.42	304.97	483.10	299.88	286.58	225.66	486.14
43	370	291.1	296.13	474.73	289.93	281.60	219.05	477.62
44	358	274.38	287.55	445.60	280.32	264.96	212.63	448.78

Table 4.9b: Rough circular load plates. Comparison of theoretical and measured bearing capacity factor N_γ.

	Terzaghi (1943)		Vesic (1973)		Meyerhof(1963)		B. Hansen(1970)	
ENSAYO Nº	Nγ Theoretical	Nγ Testing	Nγ Theoretical	Nγ Testing	Nγ Theoretical	Nγ Testing	Nγ Theoretical	Nγ Testing
45	383	338.53	304.97	551.69	299.88	326.83	225.66	555.14
46	260	287.03	218.49	471.04	204.84	278.80	160.99	472.93

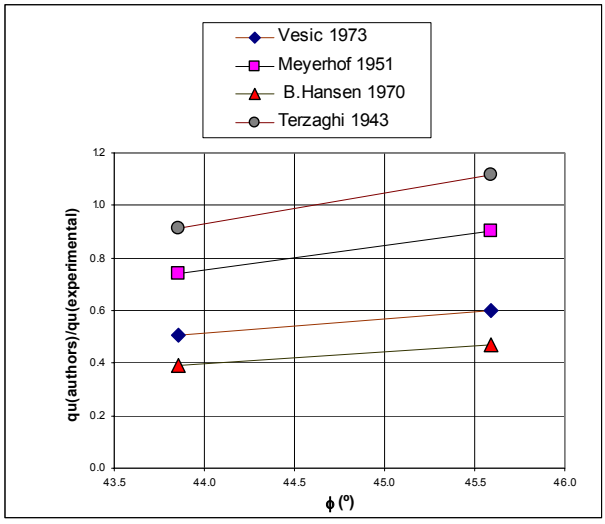

Figure 4.17: Ultimate load in rough strip footings.

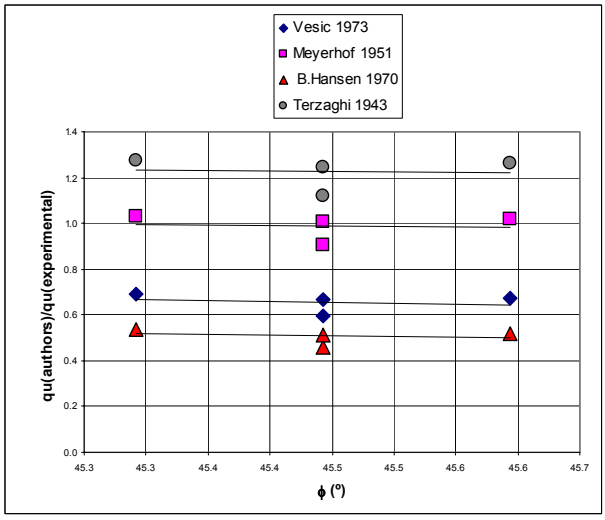

Figure 4.18: Ultimate load in smooth strip footings.

V. CONCLUSIONS AND RECOMENDATIONS

The main contribution of this thesis is to obtain a set of experimental data corresponding to tests of ultimate bearing capacity in shallow footings on a sandy soil with the purpose to analyse and compare the different existing classical theories.

As a part of the testing sequence an equipment able to form specimens of large size by the pluviation technique was designed, built and operated. Also, the readings of the loading ring and the data logging were recorded after each load increment. The footing settlements were the average of the deflections measured by the LVDT. Although, the tests were carried out on dry sand, the equipment have a drainage valve allowing in the future similar testing be done on saturated sandy soils.

The testing footings were circular rigid plates of 5, 7.5 and 10cm diameter, and a rectangular rigid plate of 6cm wide and 30cm long. The condition of smooth bottom corresponded to machined steel without any treatment to obtain a less friction. It was considered not necessary the use of oils or lubricators because in the time they can affect the testing soil. With respect to the rough surface, this was obtained by a metallic sandpaper Nº40 glued to the bottom of the testing plate.

The ratio of ultimate bearing capacity of the circular rough plates of 7.5 and 10.0cm diameter to that of smooth plates was found to be within 35% and 18.3% greater, respectively. In the case of rectangular plates the ratio of ultimate bearing capacity of rough footings was found to be 21% greater than for smooth footings.

For the type of sand tested, loading conditions and for the plates used in the investigation, it can be drawn the following conclusions

The Terzaghi's bearing capacity theory (1943) was the best fitted to the experimental evidence in all the cases analysed with rough plates. For the circular smooth

footings cases, the Vesic's theory (1973) gives the best results. And for the cases of rectangular smooth footings, the Meyerhof's theory (1963) provides the best estimation of ultimate bearing capacity. Therefore, due to the smooth case is only a theoretical supposition, the Terzaghi's theory should be the most reliable in concordance with the testing results. Nevertheless, these results are not necessary projectable to the real footings behaviour of large size due to that in these cases the greater confinement mean stress inside the pressure bulb may reduce significantly the dilatancy, in the situation of sands that tend to increase the volume when they strain by shear. The higher confinement can even yield in the failure or crushing of the soil particles.

The angle of internal friction used in the application of the classical theories above mentioned was the angle obtained from the triaxial testing. The use of the angle corresponding to the condition of plane strain, as checked, take to an appreciably overestimation of the bearing capacity. Because of the angle of internal friction in plane strain was necessary estimated in base of the formulae that appear in technical publications, it would be recommendable to carry out tests in the future that allow estimate in a more precise way the value of the angle in plane strain. Such investigation were done by Ko and Davidson (1973) and Cornforth (1964). For this purpose it should be required to design and build special testing equipment because currently there is no one in Chile. With respect to this, it is useful to know that the sand tested presents special geomechanical characteristics since the values of the angle of internal friction is greater than of commonly used sands, including for low relative densities. No measurements of critical relative densities were made. However, in the triaxial tests was noted that the sand used had a dilatant behaviour inside the range of densities used in the investigation.

With regard to the stiffness of the container, where the sand was placed and then tested, is convenient to mention the stiffness of the container was appropriate enough in the sense to avoid any influence over the bearing capacity or over the settlements measured. Each wall of the container was constructed of steel plates 2mm thick. The steel walls were held securely by welded steel grids, each composed of four 2.5cm x 2.5cm x 105cm steel runners with eight 2.5cm x 2.5cm x 65cm steel bars used as vertical spacers at 33cm centres.

Moreover, the eight steel bars connect them under the container. The stiffness of the soil container was assured to prevent the same situation experienced by Ko y Davidson (1973), i.e., the modification of the settlements measured due to the lack of stiffness of the soil container because it imparted lateral and transverse movements to the model footing during penetration.

Also, it was important to reach the enough stiffness of the reaction frame to hinder deformations that may influence in the lecture of settlements in more than 1% for the case of the largest application load. The hydraulic jack used for the tests proved to be extremely stable with no significant lateral movements either transversely or longitudinally. The vertical application of the load, without eccentricities, played a fundamental rol in the validation of the results. In fact, it was noted that the testing plate penetrated horizontally at least until the failure load. Beyond this point, in some cases the plate had a small tilt after to reach the residual load of the soil.

In the following some recommendations for bearing capacity investigations in the future are presented. First, for sand tests with relative densities larger than those here used, use sands with d_{50} greater than 0.4mm. In addition, it should be useful to test with another kind of sand, with different mineralogy and angles of internal friction. Particularly to check the validity of the theory for sands with ϕ off the range of 42º and 46º, like those here analysed. Furthermore, moisture or saturated conditions of the sand could be properly included too.

Additionally, it should be required enlarge the container's dimensions with the purpose to test greater plates. It is recommended too to carry out bearing capacity tests with different D_f. The idea is to know the real footing initial buried effect with the purpose of increase the experimental data base, so to determine more precisely the shape and depth factors of the classical theories and the size influence of the footing in the N_γ factor.

BIBLIOGRAPHY

BIEGANOUSKY, W. y MARCUSON, W. (1976) **Uniform placement of Sand**. JSMFD, Proceedings of the ASCE ,Vol. 102, N° GT3, pp. 229-233.

BISHOP, A.W. (1966) **The strength of soils as engineering materials**. Géotechnique, 16, pp. 91-128.

BOWLES, J.E. (1996) **Foundation analysis and design**. MacGraw-Hill Companies, Inc. Quinta edición. Nueva York.

DE ALBA, P., CHAN, C. y SEED, B. (1975) **Determination of soil liquefaction characteristics by larga-scale laboratory tests**. Report NºEERC 75-14, Universidad de California, Berkeley.

DE BEER, E.E. (1970) **Experimental determination of the shape factors and the bearing capacity factors of sand**. Géotechnique, 20, Nº4,pp. 387-411.

GOTTARDI, G.; RICCERI, G. y SIMONINI, P. (1994) **On the effect of footings on sand under general loads**. Proceedings of the XIII International Conference on Soil Mechanics and Foundation Engineering, Vol. III, pp. 709-712, Nueva Delhi.

GOTTARDI, G. y BUTTERFIELD, R. (1993) **On the bearing capacity of surface footings on sand under general planar loads**. Soils and Foundations JGS, Vol.33, Nº3, pp. 68-79.

GRAHAM, J. y HOVAN, J.M. (1986) **Stress characteristics for bearing capacity in sand using a critical state model**. Canadian Geotechnical Journal, Vol. 23, pp. 195-202.

HANSEN, J.B. (1970) **A revised and extended formula for bearing capacity**. Geoteknisk Inst., Bulletin 28, pp. 5-11.

HETTLER, A. y GUDEHUS, G. (1988) **Influence of the foundation width on the bearing capacity factor**. Soils and Foundation JGS, Vol. 28, N°4, pp. 81-92.

HILL, R. (1950) **The mathematical theory of plasticity**. Oxford University Press, Oxford, Inglaterra.

KO, H. Y. y DAVIDSON, L. (1973) **Bearing capacity of footings in plane strain**. JSMFD, Proceedings of the ASCE ,Vol. 99 N° SM1,pp. 1-23.

KO, H. Y. y SCOTT, R. F. (1973) **Bearing capacity by plastic theory**. JSMFD, Proceedings of the ASCE, Vol. 99 N° SM1, pp. 25-43.

KOLBUSZEWSKI, J. J. (1948) **An experimental study of the maximum and minimum porosities of sands**. Proc. 2nd ICSMFE, Vol.1, pp. 158-165.

KOLBUSZEWSKI, J. J. (1948) **General investigations of the fundamental factors controlling loose packing of sands**. Proc. 2nd ICSMFE, Vol.7, pp. 47-49.

KUMBHOJKAR, A. S. (1993) **Numerical evaluation of Terzaghi`s N_{γ}**. J. of Geotech. Engrg., ASCE, Vol. 119, N°3, pp. 598-607.

KUSAKABE, O., MAEDA, Y. y OHUCHI, M. (1992) **Large scale loading tests of shallow footings in pneumatic caisson**. J. of Geotech. Engrg., ASCE, Vol. 118, N°11, pp. 1681-1696.

LADD, R.S. (1974) **Specimen preparation and liquefaction of sands**. JSMFD, Proceedings of the ASCE ,Vol. **100** N°10, pp. 1180-1184.

LADD, R.S. (1978) **Preparing test specimens using undercompaction**. Geotechnical Testing Journal, GTJODJ, Vol 1, Nº1, pp. 16-23.

LAUE, L. (1998) **Settlements of shallow foundations subjected to combined static and repeated loading**. Proceedings of the XVI International Conference on Soil Mechanics and Foundation Engineering, Vol. III, pp. 1003-1007, Hamburgo.

LEE, S.H., CHUNG, C.K. y KIM, M.M. (1998) **The optimum instalation angle of reticulated root piles**. Proceedings of the XVI International Conference on Soil Mechanics and Foundation Engineering, Vol. III,pp. 1103-1106, Hamburgo.

LUNDGREN, H. y MORTENSEN, K. (1953) **Determination by the theory of elasticity of the bearing capacity of continuous footing on sand**. Proceedings, 3rd International Conference on Soil Mechanics and Foundation Engineering, Vol. I, pp. 409-412.

MEYERHOF, G.G. (1951) **The ultimate bearing capacity of foundations**. Géotechnique, 2, pp. 301-332.

MEYERHOF, G.G. (1963) **Some recent research on the bearing capacity of foundations**. Canadian Geotechnical Journal, Vol. 1, pp. 16-31.

MULILIS, P., CHAN, C. y SEED, B. (1975) **The effects of method of sample preparation on the cyclic stress-strain behavior of sand**. Report NºEERC 75-18, Universidad de California, Berkeley.

PERAU, E. W. (1997) **Bearing capacity of shallow foundations**. Soils and Foundations JGS, Vol.37, Nº4, pp.77-83.

PASSALACQUA, R. (1991) **A sand-spreader used for the reconstitution of granular soil models**. Soils and Foundations JGS, Vol.31, Nº2, pp. 175-180.

SAWICKI, A., SWIDZINSKI, W. y Zadroga, B. (1998**) Settlement of shallow foundation due to cyclic vertical force**. Soils and Foundations JGS, Vol.38, Nº1, pp.35-43.

SELIG, E.T. y McKEE, K.E. (1961) **Static and dynamic behavior of small footings**. ASCE Journal of the Soil Mechanics and Foundation Division, Vol. 87, Nº6, pp.29-47.

SOKOLOVSKI, V. V. (1965) **Static of granular media**. Traducido del ruso por K. Lusher, Pergamon Press, Londres, Inglaterra.

SOKOLOVSKI, V. V. (1960) **Static of soil media**. Segunda edición Traducido del ruso por D.H. Jones y A.N. Shofield, Butterworths Scientific Publications, Londres, Inglaterra.

TATSUOKA, F., OCHI, K., FUJII, S. y OKAMOTO, M. (1986) **Cyclic undrained triaxial and torsional shear strength of sands for different sample preparation methods**. Soils and Foundations JSSMFE, Vol. 26, Nº3, pp. 23-41.

TATSUOKA, F., OKAHARA, M., TANAKA, T., TANI, T., MORIMOTO, T. y SIDDEQUE, M. S. (1991) **Progressive failure and particle size effect in bearing capacity of a footing on sand**. ASCE Geotech. Special Publication, Nº27, pp. 788-802.

TERZAGHI, K. (1943) **Theoretical Soil Mechanics**. John Wiley & Sons, Inc., New York.

TERZAGHI, K. y PECK, R.B. (1967) **Soil Mechanics in Engineering Practice**. Segunda edición, John Wiley & Sons, Inc., New York.

UENO, K., Miura, K. y Maeda, Y. (1998) **Prediction of ultimate bearing capacity of surface footings with regard to size effects**. Soils and Foundations JGS, Vol.38, Nº3, pp.165-178.

VAID Y. P. y NEGUSSEY D. (1984) **Relative density of pluviated sand samples**. Soils and Foundations JGS, Vol.24, Nº2, pp. 101-105.

VERGHESE, Ch. (1972) **Bearing capacity theory from experimental results**. ASCE Journal of the Soil Mechanics and Foundation Division, Vol. 98, Nº12, pp.1311-1324.

VESIC, A.S. (1973) **Analysis of ultimate loads of shallow foundations**. ASCE Journal of the Soil Mechanics and Foundation Division, Vol. 99, Nº1, pp. 45-73.

WALKER B. P. y WHITAKER T. (1967) **An apparatus for forming uniform beds of sand for model foundation tests**. Géotechnique, 17, pp. 161-167.

ZADOROGA, B. (1994) **Bearing capacity of shallow foundations on non-cohesive soils**. J. of Geotech. Engrg., ASCE, Vol. 120, Nº11, pp. 1991-2008.